TAMPEREEN TEKNILLINEN YLIOPISTO
TAMPERE UNIVERSITY OF TECHNOLOGY

DENIS SURMANN

NLOS MITIGATION TECHNIQUES IN GNSS RECEIVERS BASED ON LEVEL CROSSING RATES (LCR) OF CORRELATION OUTPUTS

Master of Science Thesis

Examiners:
Associate Professor Dr. Elena-Simona Lohan
Prof. Dr. Jari Nurmi
Examiner and topic approved by the council of the Faculty of Computing and Electrical Engineering on 4 June 2014

Abstract

TAMPERE UNIVERSITY OF TECHNOLOGY

SURMANN, DENIS: NLOS mitigation techniques in GNSS receivers based on Level Crossing Rates (LCR) of correlation outputs
Master of Science Thesis, 89 pages, 2 appendices (5 pages)
August 2014
Examiners: Associate Prof. Dr. Elena-Simona Lohan and Prof. Dr. Jari Nurmi
Keywords: Level Crossing Rate (LCR), Multipath detection, Non-Light-of-Sight (NLOS)

Global Navigation Satellite Systems (GNSS) provide navigation services with a highly precise estimation of the position. First military influenced, the use of satellite-based positioning has gained a lot of interest also in civilian tasks nowadays. Because the GNSS performance has been improved over the years, the state-of-the-art GNSS navigation does include indoor positioning and moving autonomously with help of GNSS. The accuracy, which essentially has to be high, can be disturbed by multipath (e.g. diffraction, reflection, refraction or scattering). A possibility to detect multipath, and possibly to avoid those signals in the position solution, is totally necessary. A non-direct signal, namely Non-Light-of-Sight (NLOS), can lead to low accuracy of the positioning.

Therefore, this thesis is dealing with the NLOS detection by using the Level Crossing Rate (LCR), which has been used in electronic communication such as Wifi. The thesis is divided in two parts, including a literature review part, following by a simulation of the developed detection technique. All basic knowledge about this work can be extracted from the literature part. In the simulation section, several tests will be provided, done by Matlab® simulations. To perform a realistic GNSS signal, a dynamic Galileo Composite Binary Offset Carrier (CBOC) signal was produced.

Preface

This Master of Science thesis had been done in the Department of Electronics and Communication Engineering in Tampere University of Technology, Tampere/Finland between the middle of April 2014 and the end of August 2014.

I am very thankful to Dr. Elena-Simona Lohan as my supervisor. Even if she has not been in Tampere physically, I am grateful to her for having an open ear every time and useful discussions. She gave me professional advices and let me work on my own at the same time by evaluating my progress in working objectively.
I also would like to say thank you to my second supervisor in Tampere, Prof. Dr. Jari Nurmi, to be part of his research group.

Thank you especially to my supervisor Prof. Dr. Bernd Eissfeller. I am so grateful to him, because of creating the contact with my supervisors in Tampere and making it possible to experience my thesis abroad.
I also would like to give thanks to Dr. Jong-Hoon Won as my second supervisor in Munich.

At least, I have to say thank you to people, who believed in me, supported me and were by my side in my whole aerospace engineering study.
Thank you my comrades and truly friends Mari, Michi, Schro0 and Urbi. Thanks to my best friend Domme, who stayed so much in contact with me, even if the big distance between us was not easy at all.
Thank you mum and dad, thank you my lovely sister. You made me to that person I am and you are responsible for being successful in my life. I love you.

Martina, I love you and I am so thankful to you being by my side in every situation and truly loved and behaved me and never give up in believing in me.

Tampere, Finland, August 2014
Denis Surmann

Contents

List of Figures

List of Tables

List of Abbreviations

ACF	Auto-Correlation Function
AltBOC	Alternate Binary Offset Carrier
AFD	Average Fade Duration
AOA	Angle Of Arrival
AOD	Average Outage Ratio
ARNS	Aeronautical Radio Navigation Services
AWGN	additive white Gaussian noise
BOC	Binary Offset Carrier
BPSK	Binary Phase Shift Keying
CBOC	Composite Binary Offset Carrier
CCF	Cross Correlation Function
CDMA	Code Division Multiple Access
CNR	Carrier-to-Noise-Ratio
CosBOC	cosine-BOC
CS	Commercial Service
DLL	Delay Lock Loop
DOP	Dilution Of Precision
E	Early correlator
EGC	Equal Gain Combining
EML	Early-minus-Late
FLL	Frequency Lock Loop
GEO	Geostationary Earth Orbit

GLONASS	GLobal Orbiting NAvigation Satellite System
GNSS	Global Navigation Satellite System
GPS	Global Positioning System
GSC	Generalized Selection Combining
HRC	High Resolution Correlator
L	Late correlator
LCR	Level Crossing Rate
LCRE	Level Crossing Rate Estimation
LOS	Light-of-Sight
MBOC	Multiplexed Binary Offset Carrier
MEO	Middle Earth Orbit
ML	Maximum Likelihood
MLE	Maximum Likelihood Estimation
MRC	Maximal Ratio Combining
MSE	Mean Square Error
NCO	Numerically Controlled Oscillator
nEML	narrow Early-Minus-Late
NLOS	Non-Light-of-Sight
OPP	Outside Peak Point
OS	Open Service
P	Prompt Correlator
PDF	Probability Density Function
PLL	Phase Lock Loop
POA	Phase Of Arrival
PP	Peak Point
PRN	Pseudo Random Noise
PRS	Public Regulated Service

PSD	Power Spectral Density
PVT	Position, Velocity and Time
RHCP	Right-Hand Circularly Polarized
RNSS	Radio Navigation Satellite Services
RMS	Root Mean Square
RSS	Received Signal Strength
RSSI	Received Angle Strength Indicator
RSSML	Reduced Search Space Maximum Likelihood
SAR	Search And Rescue
SinBOC	sine-BOC
SIR	Signal-to-Interference-Ratio
SNR	Signal-to-Noise-Ratio
TDOA	Time Difference Of Arrival
TK	Teager Kaiser
TOA	Time Of Arrival

List of Symbols

$\otimes$	Convolution operator
$\cup$	Union operator
$card$	Cardinality
α	Marginal kurtosis
α_D	Composite amplitude if the desired signal power constrained
α_I	Amplitude of the co-channel interferes
α_l	Amplitude of the l^{th} signal
β_c	Critical elevation angle
$\gamma(x)$	Value of the normal distribution at the number of crossings x
γ_b	Threshold of the benchmark test
δ_{LCR}	Changing rate threshold
δ_t	Clock bias
$\delta/t)$	Dirac Pulse function
Δf	Frequency search resolution
Δ_{nEML}	Early-Late chip spacing for nEML
ϵ_i	Distance measurement error
ϵ_k	Correlation error
ϵ_ρ	Error of the contaminated signal
$\hat{\Theta}$	Estimator of phase
Θ_l	Phase of the l^{th} signal
λ	Threshold level of LCR
λ_b	Threshold level of the maximum peak width
λ_{th}	nth crossing rate of SIR process
μ	Mean of the LCR-crossings in a certain CNR
μ_{xi}	Threshold value of normalized Rayleigh-ness test
μ_R	mean of the Rayleigh-ness test
μ_{LOS}/μ_{NLOS}	Means of error in distance measurement ϵ_i of LOS/NLOS

ρ	Pseudorange
σ	Parameter of the normal distribution based algorithm
$\left[\widehat{\sigma_k^2}\right]_i$	Estimated variance of L TOA measurements and $k^(th)$ transmitter, i^{th} hypothesis
${\sigma^2}_{LOS}/{\sigma^2}_{NLOS}$	Variance of error in the distance measurement ϵ_i of LOS/NLOS
$\widehat{\tau}$	Estimated code delay
$\widehat{\tau}_d$	Estimated code phase
τ_{max}	Maximum peak in ACF
b_n	n^{th} complex symbol data
$c_{k,n}$	k^{th} chip corresponding to the n^{th} symbol
D_{nEML}	Discriminator function of nearly Early-minus-Late Correlator
E	Average detection probability
f	Multiplier
f_c	Spreading code rate
$f_{carrier}$	Carrier frequency
f_d	Doppler shift
$\widehat{f_d}$	Estimated Doppler frequency
f_{sc}	Subcarrier frequency
$F(r)$	Values below LCR threshold
H_0	Out-of-sync case for Rayleigh-ness test
H_1	In-sync case for Rayleigh-ness test
H_l	Hypothesis LOS
H_n	Hypothesis NLOS
K_{tot}	Total number of samples in correlation window
L	Number of TOA measurements
N_{BOC}	BOC modulation order
N_C	Coherent integration time
$N(r)$	Crossing rates of LCR
N_S	Oversampling factor
$p_{1,2,3,4}$	Detected probability of 1-4 paths
$p_{\dot{r},r}(\dot{r},r)$	PDF function of received signal and it's derivative
$p_{T_{B_1}}$	Rectangular pulses of amplitude 1
$P(H_l)$	Prior probability of LOS
$P(H_n)$	Prior probability of NLOS

P_c	Critical points on map aiding
P_m	Measured points on map aiding
Q	Quadrature component
r	Received signal
$\dot{r}$	Derivative signal with respect to the time
R	Average of non-coherent correlation function
$\overline{R}_k$	Normalized non-coherent correlation function
R_k	Gaussian model
s_D	Received signal power threshold
s_{th}	nth signal power crossing
S_i^{LOS}	LOS situation under i^{th} hypothesis
S_i^{NLOS}	NLOS situation under i^{th} hypothesis
S_F	Spreading factor
$S_{SinBOC}(t)$	SinBOC signal waveform
$Sign(.)$	Signum operator
$t_{k,i}$	Time measurement with the i^{th} hypothesis and k^{th} transmitter
T_C	Chip period
T_{coh}	Coherent integration time
w	Amplitude weight factor
W	Correlation window in chips
$z^{(k)}$	Sample of non-coherent CCF

1 Introduction

The efforts to develop a satellite-based navigation had been started in the 1970s by the United States (U.S.) Department of Defense (DoD). The first concept, which was affected and introduced by the military, was dealing with an autonomous GEO-orbital placed constellation. Once the Global Positioning System (GPS) has been fully operational in space by USA, other countries have started to investigate more in this research field. After the end of the Cold War, that was one of the major reasons to develop a sufficient all-weather positioning facility, the civil use became more important. First, mostly used for planes, another civil mass market grew up, such as, for example, car navigation. Nowadays, every cellphone has an integrated Global Navigation Satellite System (GNSS) chip. Europe's trial of acting autonomously, providing a navigation system, started with the Galileo program. The Galileo project is financed by the European Union (EU) and a cooperation with the European Space Agency (ESA).

Due to the technical development and the aspiration to increase the quality of GNSS services, the accuracy is a key requirement. Basically, the satellite navigation is based on measuring time and then calculating the distance between the satellite and receiver.

The accuracy does not only depend on hardware, such as the used antenna and front-end filters. The digital signal processing inside the receiver also has an deep impact on accuracy and accompanying all stages from the point of first fixing a satellite, to calculating the position solution. A crucial role in locating the position is played by the code acquisition and tracking. Acquisition takes place in order to find the visible satellites and then to estimate the code delay τ and Doppler shift f_d. Afterwards, the tracking can be done.

Different effects, such as a low signal power, characterized by Carrier-to-Noise-Ratio (CNR), are leading to a decrease of the accuracy. Besides low CNR environments (e.g. urban areas, indoors), the multipath propagation has a big influence on the performance. In general, a non-direct signal is delayed by, for example, reflection or scattering when having multipath. In case of big delays, such disturbed signal might be detected by feedback loops. In the receiver, a stored

Pseudo Random Noise (PRN) is compared to the incoming signal. An Auto-Correlation Function (ACF) is used, which is calculated based on an incoming signal and the stored PRN code, by shifting the stored code chip per chip over the incoming code. The higher the correlation between the two signals, the higher the peak of the ACF.

The classical feedback loop is known as Delay Lock Loop (DLL). But this feedback delay estimator fails to deal with multipath propagation. Therefore, newer developments with this correlator have been done, by, for example, narrow Early-Minus-Late (nEML), Double Delta ($\Delta\Delta$) or High Resolution Correlator (HRC). While the normal Early-minus-Late (EML) shifts the generated code $\pm$ 0.5 chips, the idea is to decrease this window. Caused by the possibility to use small correlation windows, current correlators can detect severe multipath.

Close to this research field of multipath detection and estimation, the literature is separating the multipaths into direct signals, known as Light-of-Sight (LOS), and non-direct signals, namely Non-Light-of-Sight (NLOS). The receiver detects a mass of signals of one satellite by multipaths at the same time, but only one has a direct path. Because the satellite is not directly visible to the receiver in NLOS environments, only non-direct signals reach the antenna. An use of such, under LOS wrongly detected, signals create an enormous error in positioning. Moving autonomously is only one example, which is forcing the idea of having the need to detect and mitigate the NLOS components. Once the NLOS is detected, either the signal can be avoided for the estimation of the position, or current advanced mitigation techniques can be implemented to use such non-direct signals without a significant loss of the accuracy.

The need of multipath detection is totally necessary for future programs with use of GNSS. Therefore, this thesis is dealing with multipath detection in NLOS environments. The objective is to design a suitable method with such complex circumstances and to evaluate it. Consisting of two major parts, the research methodology is about the developing of the NLOS or multipath detection technique with help of the Level Crossing Rate (LCR) and then testing it by computer simulations, which had been done by Monte Carlo simulation and random used parameters to form the signal naturally.

Hence, the contribution of this thesis is to develop a multipath detection technique in low CNR scenarios. Additionally, an overview of certain fields of GNSS had been done. By having a first look to general GNSS applications, the baseband process in the receiver will be described, with the main focus on multipath and NLOS estimation. Afterwards, the thesis describes the use of LCR besides its use

in the developed detection technique.

The following chapters are structured as following:

Chapter 2 is about the basic fields in satellite-based positioning, focusing on Galileo and having an overview about operating systems.
Chapter 3 presents the fundamental baseband processes in GNSS receivers.
Chapter 4 provides the detection of multipath and NLOS.
Chapter 5 is dealing with the major part about the LCR. The general application and the use of it in NLOS detection will be figured out.
Chapter 6 describes the simulation model.
Chapter 7 includes the general LCR implementation by having a closer look to improvements.
Chapter 8 is the evaluation part of this thesis, dealing with tests in different situation and fixing used parameters.
Chapter 9 presents the end of this thesis by providing a conclusion and a brief discussion about future research and open issues.

2 Basic information

This chapter handles some general information about the position measurements by a satellite-based system. This thematic has become more important over the last decades and has a big influence on our daily life. Well known systems, such as GPS and Galileo, strikingly increased the precision of positioning.

2.1 Satellite based positioning

The use of GNSS allows a high availability of navigation all over Earth (figure 2.1). Our current daily life could not work without because of its highly dependence on technical-based systems. The current task fields had changed, the idea of moving autonomous for example forces the development with respect to the accuracy[1].

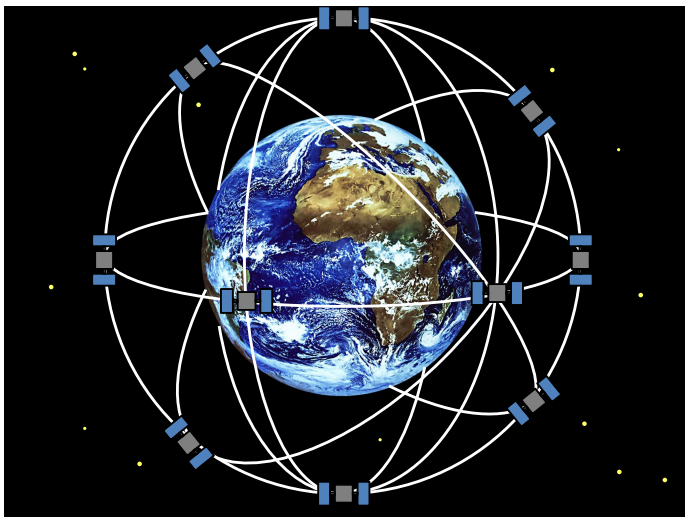

Figure 2.1: Principle of a satellite-based positioning system [2]

The idea behind the satellite-based positioning is based on a simple physical principle. Four satellites are necessary at least to determine the position. One is used to solve the clock error, the three left quantify the distance between the satellites and the receiver. In practice, even more satellites may be available and

the accuracy can be increased in such situations. Due to that reason, orbital tracks of operating systems such as GPS were chosen to ensure availability and in consequence of that, to improve the positioning accuracy. Using mostly a Middle Earth Orbit (MEO), it is possible to cover the Earth's surface by only 24 satellites. But there are also some issues supporting a Geostationary Earth Orbit (GEO), concerning some special applications.

At the receiver, the time in which the signal passes the path between the satellite and the receiver is precisely estimated. The pseudorange (ρ) is utilized to get the distance via the multiplication of time and velocity of light. The signal of the satellites contains the coarse track and the velocity of the satellite by the almanac data and the exact track by the ephemeris data. From this knowledge about tracks and distances between the satellites and the receiver, the positioning is achievable. After the acquisition, the position of each satellite, i, can be shown with the vector $r_i = [x_i\ y_i\ z_i]^T$. The position of the unknown mobile is defined by $r_u = [x_u\ y_u\ z_u]^T$. Now it is possible to create the pseudorange by adding a clock bias δ_t and an error ϵ_ρ because of a contaminated received signal [3]:

$$\rho = |r_i - r_j| = \sqrt{(x_i - x_u)^2 + (y_i - y_u)^2 + (z_i - z_u)^2} + c\delta_t + \epsilon_\rho \qquad (2.1)$$

The reason of talking about "pseudo"range is due to the receivers clock-offset, which is in theory the same for all three needed satellite signals. Usually, that time error is mostly estimated by the fourth satellite. But the use of more than four satellites is necessary to enhance the accuracy. Furthermore, the signal is moving with velocity of light , which is nearly 300.000 km/h. A time accuracy of one nanosecond (10^{-9}s) means a distance accuracy of 0.30m, which leads to the conclusion, that the time needs to be determined very precisely.

Further parasitic errors are existing and must be mentioned. The stretched tetrahedron by the satellites and the receiver should have a big volume, which can be namely described by the feature of Dilution Of Precision (DOP). The shallower the elevation (the angle between the receiver's horizontal plane and the satellite), the more precision for positioning is possible (see figure 2.1). By supposing a similar aperture angle α for two satellites, the produced area of two signals, which are reaching the receiver, depends on the elevation angle.

Another aspect is, that the signals from satellites are always influenced by the passing medium, which is mostly the atmosphere, consisting for example of Ionosphere and Troposphere. While crossing different kind of layers, the signal is delayed. The delay through the ionospheric layer is related to the signal's frequency,

while the delay through the tropospheric layer is frequency-independent. Signals of a satellite with a higher elevation are less disturbed, because the way through the atmosphere (see figure 2.2) is smaller than from satellites with a lower elevation. But in fact of the previous mentioned DOP, a higher elevation is to be needed.

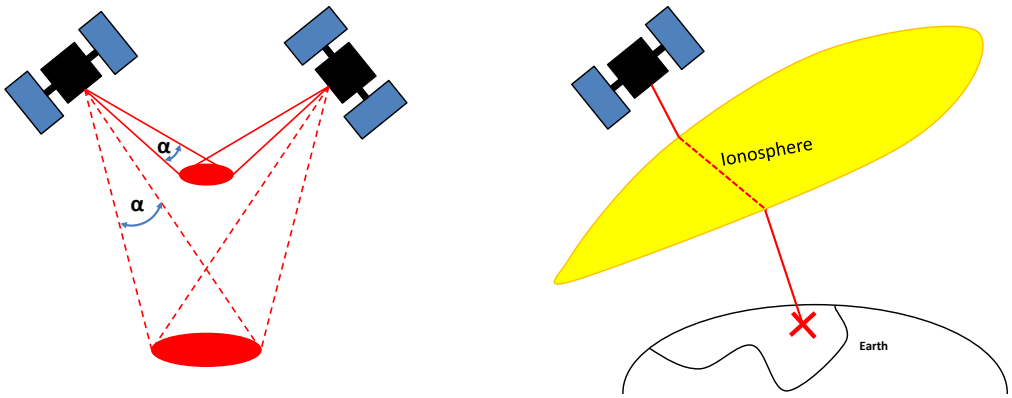

Figure 2.2: Parasitic effects in positioning - left: Illustration of DOP, where the upper circle is more precise than the circle below by having the same aperture angle α. right: An error occurs in process caused by Ionosphere [4]

The last error, that is discussed in here is about the multipath. Whenever the receiver has a non-direct (NLOS) instead of a direct signal (LOS), but it is able to receive a signal from such satellites, there are some multipaths. The multipath is a form of, for example, reflection and it should be prevented by knowledge of this as it will be explained in chapter 4.

Positioning is a complex field with respect to the presence of influencing sources (see table 2.1) and in therefore occurring positioning errors. In reality, the joint effect of these aspects has an impact on the accuracy.

Table 2.1: Errors in accuracy due to different effects, according to [5]

Source	Time Error [ns]	Positioning Error [m]
Satellite Track Error	6-60	0-1.5
Time Shift	0-9	0-1.5
Ionosphere	0-180	0-90
Troposphere	0-60	0-10

2.2 Overview of GNSS systems

Nowadays, a lot of GNSS systems are operating in orbit. The idea of common services is to offer a public and regulated services, that includes generally accessible and encoded more precise positioning (Galileo services in section 2.3). Important operational satellite-based systems are listed in following table 2.2:

Table 2.2: GNSS overview

	GPS [6][7] [8]	Galileo [8][9]	Compass [8][10]	Glonass [8][10]
Country of origin	United States	European Union	China	Russia
Year of commissioning	1990	2006	2000	1982
Current no. of satellites	32	6	15	29
No. of satellites in full constellation	32	27 + 3	25	N/A
Orbit above Earth [km]	20180	23222	21150	19130
Orbit inclination [°]	55	56	55	64.8
Satellite speeds [km/s]	3.9	3.6	3.7	3.95
Multiple access techniques	CDMA	CDMA	CDMA	FDMA, CDMA, TDMA
Main modulation types	BOC, BPSK, MBOC	BOC, BPSK, MBOC	BPSK, MBOC	BOC, BPSK, QPSK
Pilot channels	only in modernized GPS	yes	possible	yes

2.3 Galileo

The positioning system Galileo is Europe's initiative for a state-of-art GNSS project. As in straight competition to the American GPS [11], the Russian GLobal Orbiting NAvigation Satellite System (GLONASS) [12] and the Chinese COMPASS/BeiDou [13], Galileo is an attempt to operate independently, but compatible with the other GNSS. The officials propagate a global service which will work highly accurate and under civilian control. At the end of August 2014, four satellites had been placed in the MEO, two satellites were in a wrong orbit, and the first Galileo-only position fix was received in 2013 [14].

The European Navigation System will contain 30 satellites, which will be separated in three orbital plains with an inclination of 56 degrees. Each of them will orbit Earth in the Walker-Delta (27/3/1).

Generally, Galileo is going to offer high accuracy of positioning. A lot of modern techniques make sure that the operation is successfully. Some points from the official arrangement are [15], [9]:

- Galileo is going to have four services including Open Service (OS), Commercial Service (CS), Public Regulated Service (PRS) and Search And Rescue (SAR).
- Galileo aims at achieving a higher accuracy than GPS.
- To avoid errors in the receiver's processing, a "integrity message" may be part of the signal.
- The combination of GPS and Galileo, if needed , will ensure a higher availability and accuracy.

2.3.1 Galileo signal characteristics

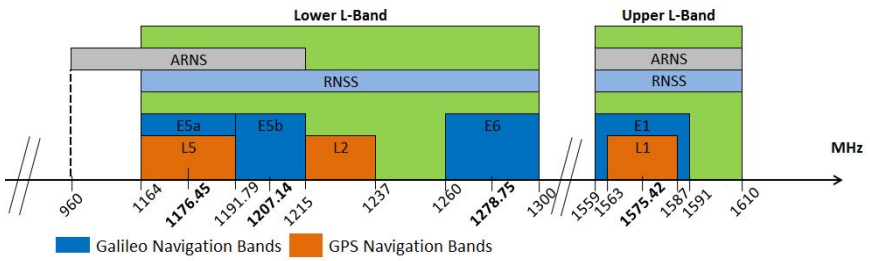

Figure 2.3: The Galileo frequency plan including the GPS-signals [9]

Galileo supports five frequency bands, which are defined in table 2.3. The E5 band contains E5a and E5b.

Table 2.3: Carrier frequency per signal of Galileo. E5a and E5b are part of the full E5 bandwith [9]

Signal	Carrier Frequency [MHz]	Receiver Reference Bandwith [MHz]
E1	1575.420	24.552
E5	1191.795	51.150
E5b	1176.450	20.460
E5b	1207.450	20.460
E6	1278.750	40.920

The use of several services in a nominal frequency is possible due to the Code Division Multiple Access (CDMA). Additionally, the signal of Galileo possesses a Right-Hand Circularly Polarized (RHCP) orientation. With respect to figure 2.3, the frequency bands were chosen inside the spectrum of the Radio Navigation Satellite Services (RNSS). Equally, all bands, except E6, are in the allocated spectrum for the Aeronautical Radio Navigation Services (ARNS).

2.3.2 Modulation types

The European GNSS is using the Binary Offset Carrier (BOC) modulation, which was introduced during the modernization of GPS. The idea behind is to spread the band and its effect is a replaced bandwidth, that is further split from the central carrier frequency [9], [16]. An overlapping with the C/A or P(Y)-Code does not take place. Galileo is transmitting a data-less signal within the pilot channel besides the data signal. Because of the fact, sending an "empty" PRN, the acquisition and tracking processes can be done more easily. Navigation data are unknown for the receiver at the first time to fix. Data-less channels are providing some advantages, such as the need to estimate a lower number of parameters than in data channels. This may ensure a faster tracking of the satellites [9], [16], [17].

Generally, BOC modulated signals are characterized in two ways. BOC(f_s, f_c), where f_s is the subcarrier frequency and f_c the spreading code rate. And sometimes BOC(n,m) is used in literature with:

$$n = \frac{f_s}{f_{ref}}[MHz] \tag{2.2}$$

$$m = \frac{f_c}{f_{ref}}[MHz], \quad f_{ref} \text{ is equal to 1.023 MHz.} \tag{2.3}$$

Galileo supports different kind of BOC-types in service. One is known as Alternate Binary Offset Carrier (AltBOC) for the E5 signal. This modulation splits the spectrum around its carrier frequency. All sidebands contain two PRN. The signal is divided in two components, the pilot (E5aQ, E5bQ) and the in-phase (E5aI, E5bI) components.

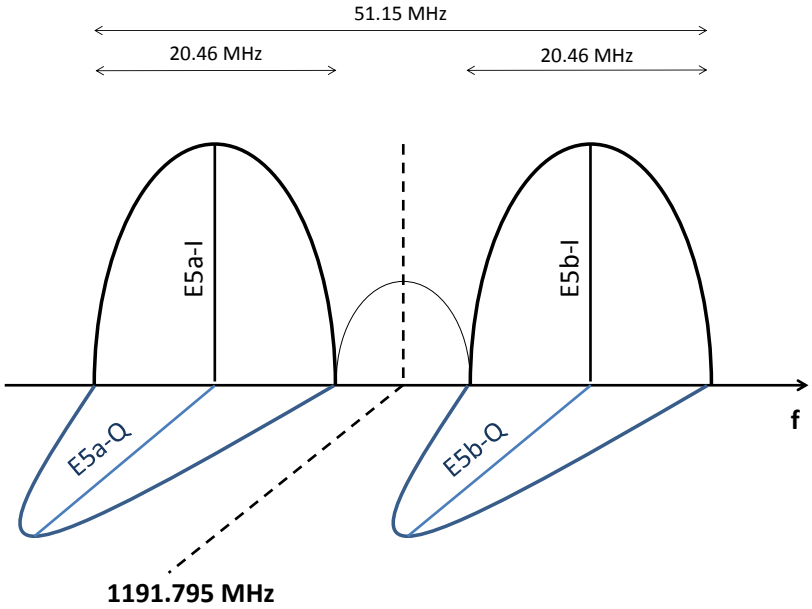

Figure 2.4: Galileo AltBOC E5 with pilot (Q) and in-phase (I) components [17]

In case of Galileo, the important part is about the sine-BOC (SinBOC). Just for completing the information, some other relevant variant is named cosine-BOC (CosBOC). An interested reader can read through [18], [19] and [20]. The previously mentioned SinBOC time waveform can be easily shown by following equation 2.4 [20].

$$s_{SinBOC}(t) = sign\left(sin\left(\frac{N_{BOC}\pi t}{T_C}\right)\right) \tag{2.4}$$

where *sign* is the signum operator. The BOC modulation order, which is included, is given by $N_{BOC} = 2\frac{f_{SC}}{f_C}$ [21]. This signal is fully defined by two parameters, namely from the BOC modulation order (N_{BOC}) and the chip frequency (f_C),

that is $T_C = \frac{1}{f_C}$, or the subcarrier frequency (f_{sc}). The SinBOC modulated signal can be written in a similar form which is close to the form of the Binary Phase Shift Keying (BPSK):

$$s(t) = s_{SinBOC}(t) \otimes \sum_{n=-\infty}^{+\infty} b_n \sum_{k=1}^{S_F} c_{n,k}\delta(t - nT - kT_C) = s_{SinBOC}(t) \otimes c(t) \quad (2.5)$$

Equation 2.5 contains b_n as the n^{th} complex symbol data, the spreading factor S_F, T_C and T as the chip and code symbol period and the convolution operator $\otimes$ and $\delta(t)$, the Dirac Pulse function. An equivalent representation of the SinBOC that is shown in [22] is:

$$s_{SinBOC}(t) = p_{T_{B_1}}(t) \otimes \sum_{i=0}^{N_{BOC}-1} (-1)^i \delta(t - iT_{B_1}) \quad (2.6)$$

where $p_{T_{B_1}}$ is the rectangular pulse of amplitude one, T_{B_1} is equal to $\frac{T_C}{N_{BOC}}$ and the the Dirac Pulse function $\delta(t)$[22]. It can be shown, that the Power Spectral Density (PSD) is clearly defined by equation 2.7. In the event of even N_{BOC}, the equation below includes "sin". Otherwise, the use of "cos" is necessary for correct calculations [23]. The equation and illustrated graph, based on that, are shown in figure 2.5 :

$$G_{SinBOC(m,n)}(f) = \frac{1}{T_C} \left(\frac{sin\left(\pi f \frac{T_C}{N_{BOC}}\right) sin/cos(\pi f T_C)}{\pi f cos\left(\pi f \frac{T_C}{N_{BOC}}\right)} \right)^2 \quad (2.7)$$

Based on the weighted SinBOC(1,1) and SinBOC(6,1), the result is a new variant, namely Composite Binary Offset Carrier (CBOC) which is currently used in Galileo OS signals. As a modulation scheme that has been selected for the market, a specification is required. Depending on an addition or subtraction, the combination of two SinBOC is named CBOC('+') or CBOC('-') [9]. A thinkable mix can also be used by taking CBOC('+') for odd and CBOC('-') for even chips [22].

SinBOC (1,1) does function with a hold block, while matching double the rate of the SinBOC (6,1). A composition of this SinBOC can be described as:

$$s_{CBOC}(t) = w_1 s_{SinBOC(1,1),held}(t) \pm w_2 s_{SinBOC(6,1)}(t) \quad (2.8)$$

Here, the addition or subtraction is depending on what kind of CBOC('$+/-$') is in use. In equation 2.8, w_1 and w_2 are the amplitude weighting factors. Because

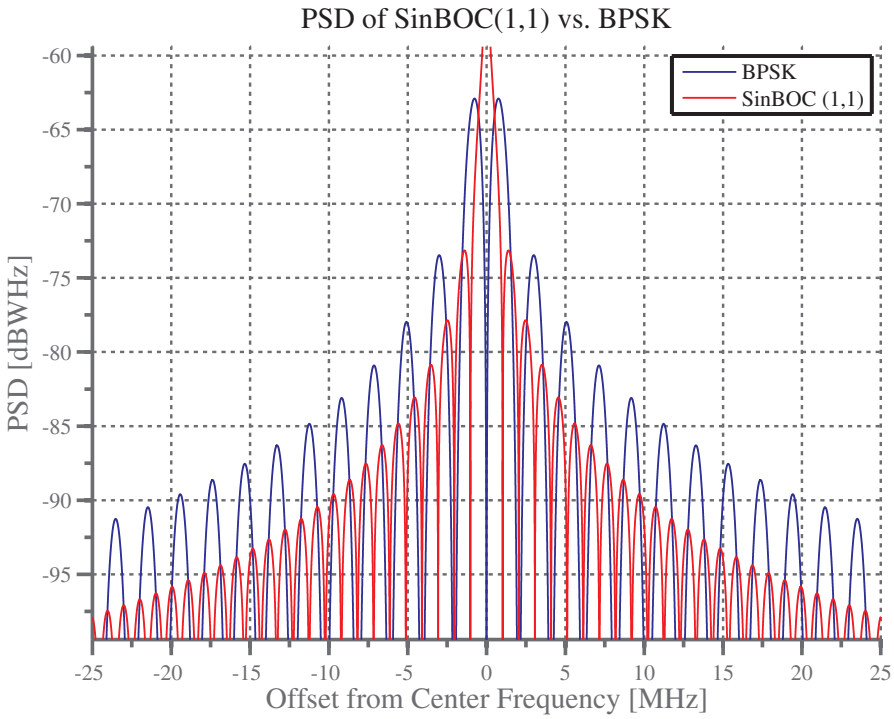

Figure 2.5: PSD of SinBOC(1,1) and BPSK

of the sum $w_1^2 + w_2^2 = 1$, the choice has to based on the PSD. Galileo for example places 50% of power for the pilot channel, thus the rest for the in-phase channel. In that case, w_1 is selected as $\sqrt{10/11}$ and w_2 with $\sqrt{1/11}$.

3 Fundamentals of GNSS Receiver operational technologies

The GNSS receiver is a navigation device which processes the incoming signal for positioning. Upcoming technologies have to handle and accurately achieve the navigation data. Hence, the procedure of processing the incoming data is an important part of positioning. Therefore, this chapter deals with some general information about the receiver from the very beginning by searching a signal, to the stage of extracting the navigation data.

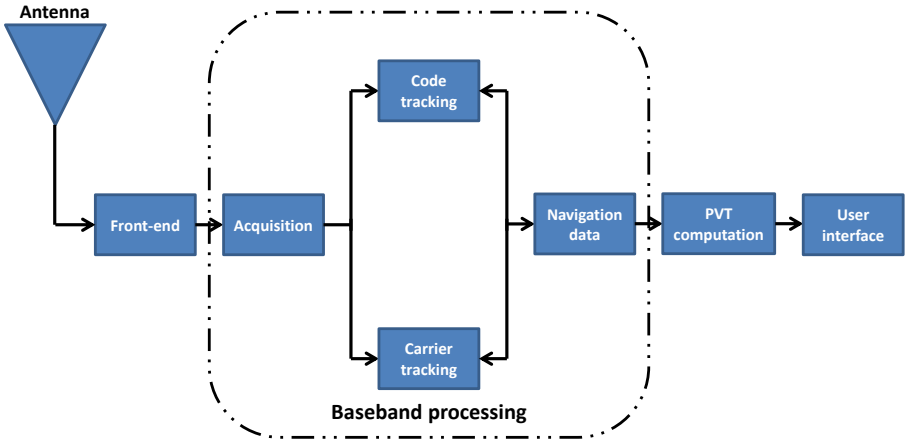

Figure 3.1: Diagram of a typical GNSS Receiver [20]

In reference to figure 3.1, the received signal from the satellite goes first through the antenna and the front-end blocks. Afterwards, once the signal is acquired, the receiver is following a tracking process and try to extract its containing navigation data to start positioning. The result is given by position, velocity and time (PVT solution). Then, the PVT is passed to an interface, which supports an user application [24].

3.1 Signal acquisition

The acquisition process extracts early information from the incoming signal. First, the receiver needs to determine which satellites are visible to the antenna. Because of the fact, that every CDMA-based GNSS transmits a unique PRN, a good separation of incoming signals is guaranteed by using specific codes, such as gold-codes for GPS [25]. The receiver does a correlation, which can be easily described as a comparison between the incoming signal and its replica, which is saved in the memory of the device. A high enough correlation peak with one PRN is an indicator, that the corresponding satellite is visible to the receiver. The result of a cross-correlation between two different PRNs would be close to zero [26]. When a signal is fixed, the receiver can estimate the code delay ($\widehat{\tau}$) and frequency ($\widehat{f_d}$) by consulting the Doppler shift (f_d), which is caused by the relative speed between the satellite and the device. The frequency band that needs to be observed is defined as $\pm$ maximum Doppler shift from the carrier frequency ($f_{Carrier}$). Hence, the rule of thumb $\Delta f = 2/(3T_{coh})$, where Δf is the frequency search resolution and T_{coh} is the coherent integration time, has to be regarded for the frequency spacings [24]. In practice, such shift is about $\pm$ 9kHz.

A separation of the searching is done by dividing the searching space into code and time bins. Depending on the search technique, the task is to find the code phase ($\hat{\tau}_d$) and frequency (f_d) in one specified cell as shown in figure 3.2 [27] [20].

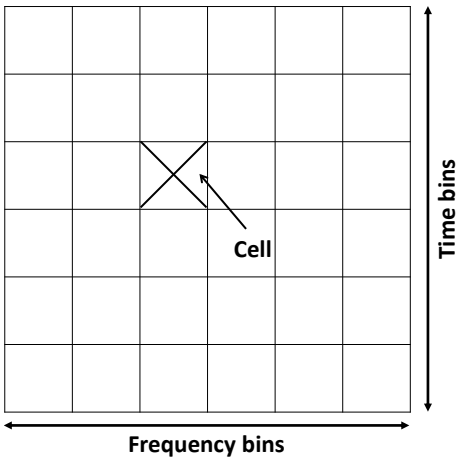

Figure 3.2: Code acquisition is a three dimensional problem, which is needed to be solved during the signal acquisition [16]

Such searching process consists of thousand of bins and there are a lot of techniques which are shown below [21] [28]:

- The **serial search** is only one bin per window, which is a multiplication between incoming signal and each search bin. Only one complex correlator is needed. Therefore, a high acquisition time, because many bins have to be searched, is the result. The acquisition time is proportional with the code epoch length [29].
- The **parallel search** contains more than one bin per window in only one window for the whole search space. This method increases the complexity highly, while decreasing the acquisition time [30].
- The **hybrid search** is a combination of serial and parallel search to achieve a better trade-off in case of the acquisition time and complexity. Several bins per window and several windows in the whole search space are used [31].

3.2 Signal tracking

In the last preceding section 3.1, the acquisition of the incoming signals was described. After completing, the receiver starts the code and carrier tracking to extract the navigation data, as shown in figure 3.1. Tracking is an important process, because the accuracy is highly depending from the code and carrier tracking.

3.2.1 Code tracking

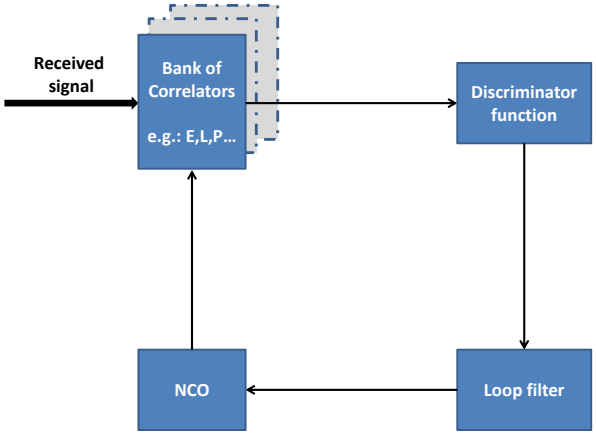

Figure 3.3: Generic block diagram of a code tracking loop [20]

The function of code tracking is to estimate the delay of the received signal as much as possible. This is done by a comparison between a generated PRN

replica, which is stored in the receiver, and the incoming delayed signal from the satellite. A correlation takes place until maximum peaks are reached. After the alignment is accomplished, the PRN can be removed. As the result, the carrier modulated navigation data are left [32].

GNSS receivers mostly use a feedback loop for code tracking. One known is the DLL, which can be seen in figure 3.3. Beneath DLL varieties, the EML is the most popular in literature. It contains three correlators, namely Early correlator (E), Prompt Correlator (P) and Late correlator (L). Commonly, the E and L are generated with a spacing of ± 0.5 chips beside the Prompt Correlator. Every incoming signal is correlated with each of these, which can be extracted in figure 3.4.

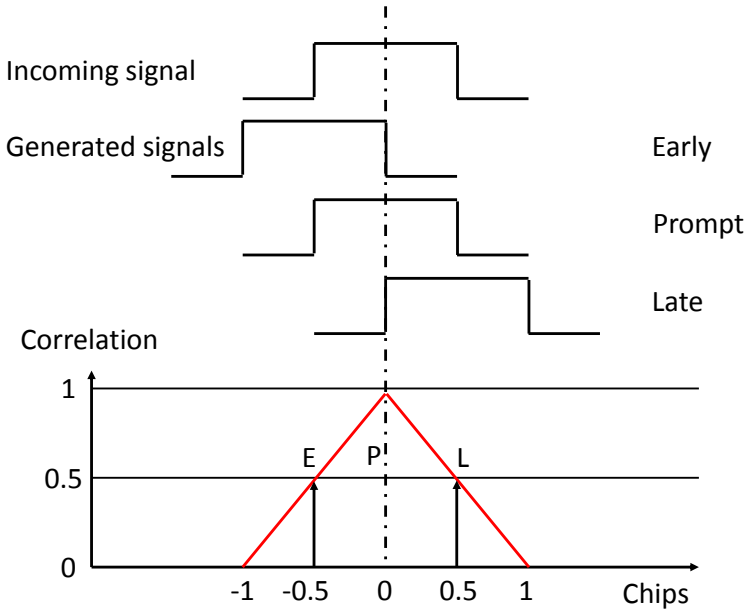

Figure 3.4: DLL principle for EML

While the normal EML uses a one chip space between the E and L correlator, the nEML supports a less wide space. The gained information is then used in the discriminator, where the gap between the incoming signal and the replica is measured by integrating the output over N_C milliseconds and then it is squared [33] [34]. Multipath is less severe near to the peak of the cross-correlation than in the away areas. The discriminator function therefore can be apprehended as:

$$D_{nEML} = E_1 - L_1 = |R(\tau + \frac{\Delta_{nEML}}{2})^2| - |R(\tau - \frac{\Delta_{nEML}}{2})^2| \tag{3.1}$$

E_1 and L_1 are the early and late delayed reference code, consisting of $R(\tau)$, the

average correlation function between the replica and the received signal with the spacing Δ_{nEML}. Double Delta ($\Delta\Delta$) is another well known DLL, which uses two correlation pairs instead of one [35]. The "wider" pair has a twice larger chip space than the "narrow" pair. As the result, the discriminator function is comparable to equation 3.1:

$$D_{nEML} = a(E_1 - L_1) - b(E_2 - L_2) \tag{3.2}$$

In the situation, where a=1 and b=$\frac{1}{2}$, the correlation names HRC[36]. By modification of a and b, the correlation is forcing the process of accuracy. The performance can be defined by the S-curve (see figure 3.5), which is visualizing the expected value of the error signal, based on a function with reference parameters (e.g.: code phase error) [37].

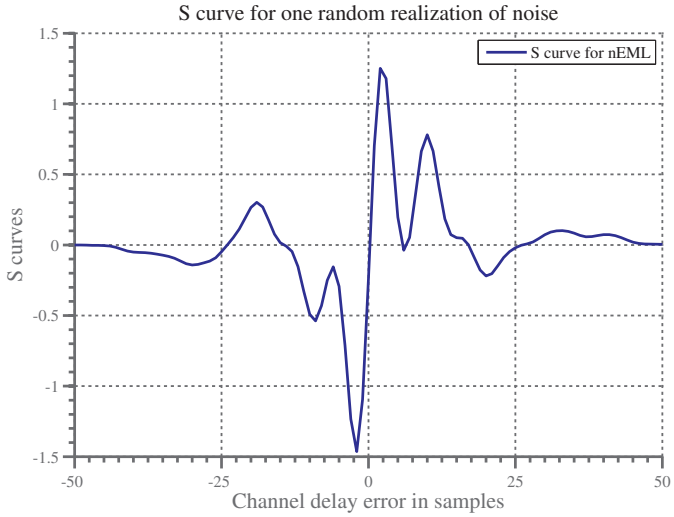

Figure 3.5: S-Curve for the nEML single path channel

At least, with regard to code tracking, the Numerically Controlled Oscillator (NCO) is fed by the output of the discriminator function, with its goal to generate a precise replica code. Beforehand, the signal passes through a loop filter, which reduces the noise and aims to produce an exact estimate for an original signal in the output.

3.2.2 Carrier tracking

Once, the code has been tracked, another important processing can be done by another feedback loop, such as the Phase Lock Loop (PLL) and Frequency Lock Loop (FLL). The PLL provides a correction of the phase, tracks and also estimates

the misalignment between the P correlator and the incoming signal. Ordinarily, the task is done by the Costas loop [38] [7]. The update is then used to remove the Doppler. The FLL supplies the frequency corrections with a generated frequency error signal. Hence, both loops achieve a better carrier tracking.

4 Advanced signal processing

In ideal situations, a GNSS receiver is able to do the positioning accurately. Even so, in reality, various error sources have an effect on the accuracy and the performance of the receiver. GNSS segments can be categorized into three categories. Depending of where they are located, literature talks about space segment related errors [39] [32], receiver related errors [20], that are described in the references, and last but not least propagation channel errors.

For propagation channel errors, the incoming GNSS signal is affected by the passed medium between the antenna of the satellite and the receiver. Concerning this high dynamic process, due to the velocity of space and user segment, the error varies during the measurement period. According to this, the following chapter discusses in detail about multipath, its analogous phenomenons and how to identify and handle such parasitic signals.

4.1 Multipath vs. NLOS

One of the most dominant error source is **multipath**. This effect is caused by shadowing, scattering, refraction and reflection for example (see figure 4.1). GNSS measurements are based on time reckoning. As the result of reflection, the transmitted signal covers a longer distance to the receiver, which evokes a delay with respect to the direct path. Possibly, the receiver detects multiple copies of the desired signal. If there is a direct path, the receiver can resolve the multipath in case of long delays. Furthermore, the size of the error might also be different, either from higher-, or lower-elevation satellites. Formerly mentioned constellation might be better for multipath errors, but worse for the accuracy with respect to the DOP as described in section 2.1 [7].

The shadowing decreases the signal power, while passing foliage or structure. In such given case, the multipath signal can be better tracked, because it is less sever than multipath signals, which are affected by reflections for example. Despite having a lower power level, multipath signals without any shadowing have just a little distortion on the direct path and consequently produce little errors.

Nevertheless, it has a direct leverage on the correlation function.

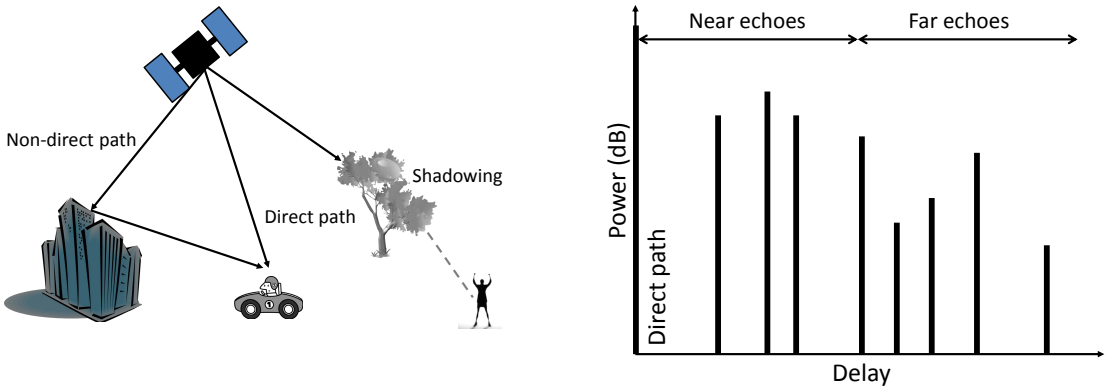

Figure 4.1: Left: Multipath example scenarios; Right: Example for a power-delay-profil

Multipath usually allows the receiver to detect a direct signal from the satellite. But **NLOS** creates much more difficult environments, in which at the receiver, it is not possible to detect a direct signal, because of geometrical circumstances. Whenever the signal is blocked by a medium (e.g. forest, inside buildings), the direct path is disturbed. Currently, NLOS becomes more and more important by reason of rising cities and the aspiration for greater mobility. In consequence of multipath, NLOS leads to an extra power loss and changing angles of incidence. Hence, to achieve an acceptable location estimation, the need to identify whether the signal comes from LOS or NLOS is totally necessary. Usually, corrupted measurements can be defined if the receiver obtains a mass of signals, when there is a propagation from a direct path. But NLOS measurements have to be reconstructed to form estimated LOS measurements [40]. The multipath detection is the main scope of the thesis, because such signals, which are wrongly detected as direct signals, cause large errors in positioning.

4.2 Basic measurements

Basically, the measurements in the receiver are based on distance and angular observations in order to support the multipath or NLOS detection. The use of such information is needed with respect to the idea of detection or mitigation:

TOA/TDOA

Measuring the time of a signal, which undergoes a distance between the transmitter and the receiver, is already known for GNSS principles. Time Of Arrival (TOA) is the absolute time measuring between those. As it was stated in section 2.1, the time synchronization and measurement must be precisely because of the signal's speed (velocity of light) [41]. Time Difference Of Arrival (TDOA) based on the same principle by adding a second transmitter. In comparison to TOA, this method allows to determine the clock bias. To increase the accuracy, more transmitters can be used.

AOA

The signal might be reflected. The result is an dynamic angle of incidence, which can be measured by the antenna array or beam forming. Namely the Angle Of Arrival (AOA) is measurable with less captures, but requires a high antenna complexity. Depending on the antenna radiation patterns, AOA can be used for multipath and shadowing detection [42].

POA

Phase Of Arrival (POA) covers the same idea such as TOA. This principle determines the absolute distance while using the incoming carrier phase. A LOS path is necessary to start this process. It starts with appraising the received signal on multiple frequencies to extenuate phase wrapping. The result of changing phases then used for the distance determination [43].

RSSI

The last principle uses the overall average of the Received Signal Strength (RSS) over a defined sample period to concludes the distance. Known as Received Angle Strength Indicator (RSSI), it uses a propagation modeling [20]. But in fact of the large distance between the satellites and the receiver and the therefore small signal strength of the signal, the RSSI is not used in GNSS.

4.3 Multipath detection

Multipath has been previously described and the detection is important for the position solution. In such a case, the receiver detects NLOS signals, which are caused by shadowing, scattering, refraction and reflection. Some detection tech-

niques will be briefly presented. Multipath can be generally detected at, for example, the antenna, signal processing and navigation level [44].

One simple detection technique is about the **3D positioning**. The multipath detection with 3D positioning can be done with a statistical threshold. Such threshold is based on a data set for several satellite signals in single or multipath cases with respect to the elevation of the satellite and the certain CNR levels. As presented in [45], a received signal is compared to the threshold to identify a presence of multipath, but multiple frequencies are required.

Another method to detect multipath can be done by **means of multi-correlators**. By means of a coherent code phase discriminator, which is defined as a linear combination of the correlator outputs, an optimum S-Curve can be determined. A suitable ACF peak, which is less distorted in single path cases, determines the presence of one-path. Extremely weak multipath signals can be identified as a NLOS environment. Therefore, a test metrics needs to be set up and compared to a threshold [46].

In case of multiple-antenna receivers, multipath might be detected by use of an **estimated spatial covariance matrix** to construct metrics. Presented in [47], the matrix is diagonal with entries related to the Gaussian noise power. In case of multipath, such matrix departs from diagonal.

The last method of multipath detection requires a **dual-polarisation antenna**. Such technique computes the CNR density from the left-hand circular polarised outputs, which then will be subtracted from the right-hand polarised part. If the results are negative, NLOS is detected. When having positive results under a certain threshold, which is based on an a direct path environment, multipath is detected.

4.4 Non-Light-of-Sight detection

NLOS detection does have the major focus in this thesis. Because of the absence of a direct path between the satellite and the receiver, the detection in such circumstances might be problematic. With respect to big measuring corruptions, NLOS needs to be detected.

4.4.1 Likelihood function

In order to differentiate LOS from NLOS situations, the distance measurement noise is usually Gaussian allocated of mean and variance. In first case, prior in-

formation are mostly available, when the measured errors are related to the CNR. Due to that necessary knowledge, NLOS situations have to be handle carefully. The Likelihood test can be used to indentify non-direct signals [48] [49]. Basically, this method is based on TOA measurements (see section 4.2)

Assuming that there are L distance measurements, the elements of the sample vector $\mathbf{r} = [r_1, r_2 \ldots r_L]^T$ are described as

$$r_i = d + \epsilon_i \tag{4.1}$$

where d is the true distance and ϵ_i the error in the distance measurement. Then, the Probability Density Function (PDF) of $\mathbf{r}$ is given by

$$p(\mathbf{r}|d,H_l) = \frac{1}{\sqrt{2\pi}\sigma_{LOS}^L} exp\left\{-\frac{1}{2\sigma_{LOS}^2}\sum_{i=1}^{L}[r_i - (\mu_{LOS}+d)^2]\right\} \tag{4.2}$$

$$p(\mathbf{r}|d,\mu_{NLOS},\sigma_{NLOS},H_n) = \frac{1}{\sqrt{2\pi}\sigma_{NLOS}^L} exp\left\{-\frac{1}{2\sigma_{NLOS}^2}\sum_{i=1}^{L}[r_i - (\mu_{NLOS}+d)^2]\right\} \tag{4.3}$$

where the values define for eq. 4.2 in LOS and 4.3 in NLOS situations under the hypothesis H_l or H_n:

- $P(H_l)$ as the known prior probability of LOS condition;
- $P(H_n)$ as the known prior probability of NLOS condition;
- μ_{LOS}/μ_{NLOS} as the means of ϵ_i;
- $\sigma_{LOS}^2/\sigma_{NLOS}^2$ as the variances of ϵ_i;

Now, the hypothesis can be characterized by the assumed LOS (S_i^{LOS}) and NLOS scenario (S_i^{NLOS}). In addiction of time, which is passed by the traveled distance, the variance of L TOA measurements is expressed as:

$$\left[\widehat{\sigma_k^2}\right]_i = \frac{1}{L}\sum_{l=1}^{2}(t_{k,i} - r_i)^2 \tag{4.4}$$

under the i-th hypothesis and the k-th transmitter, where $t_{k,i}$ is the estimated time and r_i the sample vector. [50], [51]. With use of the Maximum Likelihood (ML) algorithm and the knowledge of equation 4.4, the decision rule can be seen below:

$$\hat{i} = \arg \min_{l} \left[\ln \gamma_l^{-1} + \sum_{k \in S_i^{LOS}} \frac{L}{2} \left(\frac{\left[\widehat{\sigma_k^2} \right]_i}{\sigma_k^2} \right) \right] \tag{4.5}$$

where the constants γ_l are assigned according to each probability of the hypothesis. In summary, the idea is to compute a ML estimation of the positioning, which only uses LOS scenarios and then compare this to the theoretical variances. Whenever the hypothesis has been selected, the final and partial position estimate is corresponding.

4.4.2 Ray tracing and map aiding

In comparison to other environments, positioning in cities acquires reliable measurements, even in fields of autonomous vehicles. Therefore, a virtual image, made by a rotary camera, sensor, or a ray tracing antenna, is analysed to decide whether the detected GNSS satellite can be directly viewed nor not. Thus, a 3D model of the area must be available, containing geometrical information about all important objects (i.e. buildings, roads) [52].

Basically, the known position is compared to the direct LOS signal path with the city model. Such from NLOS are then excluded and not or less used in the position solution. Anyway, in processing, the sensor built image is analyzed to receive data about the Euclidian distance between the two closest corresponding points or pixels, and the depth of the closest points. The result is the critical elevation β_c to create a threshold, if the received signal is affected by NLOS or not:

$$\beta_c = \arctan \left(\frac{\text{distance}(P_c, P_m)}{\text{depth}(P_m)} \right) \tag{4.6}$$

where P_c are critical points and P_m are measured points. Referring to figure 4.2, the sensor tracks all critical points around the receiver with the elevation and direction. Hence, a hemisphere, with its zenith above the sensor, can be done. All satellites, which are allocated in the shaded area, are in LOS.

In order to use an urban model, a non camera or sensor based system is also possible by roughly estimate the position first, then use the stored 3D data to determine usable satellites at that time [54]. The principle is nearly the same by creating a threshold for LOS and NLOS signals and precise it over the time.

That ray tracing extracts all relevant channel parameters, characterized by POA, AOA and TOA [55]. First, a geometrical path between the receiver and the

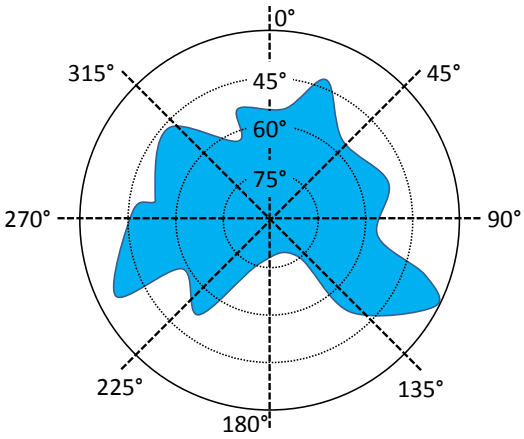

Figure 4.2: Critical elevation for LOS signals (The shaded area shows LOS visibility) [53]

satellite is searched, then physical and electromagnetic properties for each ray are calculated. Using map aiding or ray trace can highly increase the accuracy, because NLOS signals can be identified.

4.4.3 Shadow maps

Comparable with map aiding or ray tracing (subsection 4.4.2), shadow maps are also working on the same idea simply. As already mentioned before, such methods using a 3D model of all higher surrounding objects, that possibly have an effect on the satellite's visibility. In difference to map aiding or ray tracing, shadow maps contain the signal coverage for each satellite in a certain position. Therefore, buildings and other models are projected to the ground. The satellite positions must be known to start calculating with respect to the possible visibility [56].

Once, the grid of the building boundaries has been done, an initial position by GNSS or other positioning methods is acquired, to roughly define the search area. This means also to find available satellites during the acquisition. When the first position fix is done, all visible satellites, irrespective of whether they are in LOS or NLOS, are quantified under the view of the elevation and building boundary. Signals, which are probably affected by multipath, then are lower weighted in the shadow matching positioning solution [57].

4.4.4 Normalized Rayleigh-ness test

The Rayleigh-ness test tries to identify whether there is a Rayleigh-distributed random process. Such test is used to decide on possible presence of a mean μ_R

of the complex Gaussian model, that is for example $R_k = \mu_R + \epsilon_k$, where ϵ_k is the correlation error. Both contributions, Rayleigh ($\mu_R = 0$) and Rice ($\mu_R \neq 0$), can be generated. If there is a useful signal with the considered code shift, it can be defined by two hypotheses on the observed series $\Gamma = [|R_1|; ...; |R_k|]^T$, whose samples are detected at the output filter of the matched filter. They are either in an in-sync (i.e. presence signal) or out-of-sync case (i.e. absence of signal), characterized by H_1 and H_0 [58]. The testing variable is represented in below:

$$X = 2\left[\frac{1}{N}\sum_{k=1}^{N}|R_k|^2\right]^2 - \frac{1}{N}\sum_{k=1}^{N}|R_k|^4 \tag{4.7}$$

that can be expanded by adding the expression of $R_k = |\mu_R + \mathrm{Re}[\epsilon_k] + j\,\mathrm{Im}[\epsilon_k]|$ because of the receiving I/Q components of random variables. By also adding α, namely the marginal kurtosis, the mean value can be shown as below.

$$E[X] = \mu_R^4 + 2(3-\alpha)\sigma_R^4 + \frac{2}{N}\left[4\mu_R^2\sigma_R^2 + 2(\alpha-1)\sigma_R^4\right] \tag{4.8}$$

where σ_R is the variance and N the number of the observed series. One of the weakness points is caused by the argument to estimate the variance of R_k every time. The normalized Rayleigh-ness test avoids the evaluation of the variance of the received symbols. Therefore, equation 4.7 is divided by the variance of R_k. The new testing variable ξ is then:

$$\xi = \frac{\frac{1}{N}\sum_{k=1}^{N}|R_k|^4}{\left[\frac{1}{N}\sum_{k=1}^{N}|R_k|^2\right]^2} \tag{4.9}$$

The normalized test is as follows:

$$\xi < \nu_\xi \text{ for } H_1 \; or \; \xi > \nu_\xi \text{ for } H_0 \tag{4.10}$$

where ξ is the testing variable and ν the threshold value. If the testing variable is greater than ν_{xi}, the algorithm decides for H_0, otherwise for H_1. The equation 4.9 is equivalent to the ratio between the (estimated) variance of the squared correlation samples $\{|R_k|^2\}$ and the (estimated) mean of the samples [59]. For a reduction of the variance in the in-sync case, the acquisition process is supported by means the presence of the second term in the new testing variable [60].

4.5 Multipath mitigation

Multipath has already been stated as one of the most dominant error sources in section 4.1. In order to detect it, some mitigation possibilities had shown up over the last decades, caused by the interest of increasing the accuracy. State-of-the-art processing methods attempt to match the ideal correlation function to the observed function in multipath.

4.5.1 Common mitigation techniques

Conventional techniques are based on EML variations in a DLL feedback loop. The nEML, which was mentioned in 3.2.1, is the most popular mitigation technique for multipath. This is due to the easy implementation, while having a robust tracking performance. A reduce of noise and multipath is eventually possible [61]. Nowadays, a use of correlator spacings between 0.05 and 0.2 chips are common, but affected by the front-end bandwidth [62].

Another familiy of DLL variants is the $\Delta\Delta$-technique. It offers a better multipath rejection in medium-to-long delay multipath in good C/N_0 (CNR) scenarios [63]. A well known case is the HRC (section 3.2.1), which has an higher performance than the nEML. [36]. In figure 4.3, the nearest ambiguous zero crossing of the HRC is closer to the correct crossing in comparison to the nEML curve. Hence, the probability of looking to any side peaks is much higher.

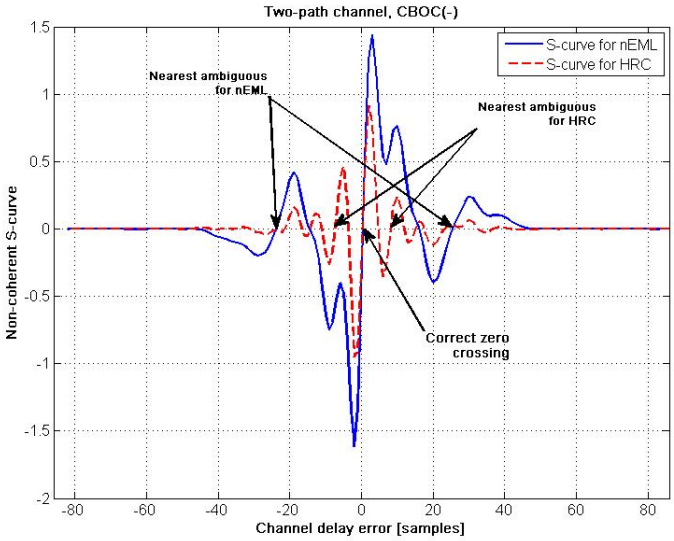

Figure 4.3: A non-coherent S-Curve for CBOC(-) in two path

4.5.2 Advanced mitigation techniques

For any GNSS signal, one of the most important parameter of interest is the LOS code delay. Conventional methods cannot follow the LOS code accurately. State-of-the-art multipath mitigation techniques mostly make use of the correlation function. An implementation of a vast number of correlators is usually required in order to estimate the channel characteristics. They are then used to mitigate the multipath effect and promise an higher accuracy.

Teager Kaiser

The Teager Kaiser (TK) technique makes use of the signal energy by the TK operator. From that output $\Psi(x(n))$ of the operator, sourced by a discrete signal $x(n)$, a presence of multipath can be detected. The non-coherent correlation can build the necessary input for a symbol n, so that the output is defined as [64]:

$$\Psi_{TK}(x(n)) = x(n-1)x^*(n-1) - \frac{1}{2}\left[x(n-2)x^*(n) + x(n)x^*(n-2)\right] \quad (4.11)$$

At least, three correlation values are needed to start TK in P, E and very E correlator. In practice, more correlators are utilized and the estimation is rather sensitive to the noise, depending on the chosen threshold [65]. Anyway, the combination of the TK and nEML aims, that the main lobe of the non-coherent correlation function is much steeper. The zero crossing for the S-curve now might be closer to the real true delay than in comparison to the use of the nEML [64]. The decision of a present multipath is done with respect to a specific threshold as the interested reader find in [66].

Reduced Search Space Maximum Likelihood Delay

Another estimator, the Reduced Search Space Maximum Likelihood (RSSML), also represents an up-to-date technique in multipath mitigation. In theory, Maximum Likelihood Estimation (MLE) describes a statistical model, which has an output of realistic estimates by given model parameters [67]. In statistics, the Mean Square Error (MSE) can be described as

$$\mathrm{MSE}(\hat{\theta}) = \mathrm{E}\left[(\hat{\theta} - \theta)^2\right] \quad (4.12)$$

where Θ is the unknown parameter and $\hat{\Theta}$ the estimator [68]. It is comprehensible, that parameters with small mean square errors are those, which maximizes

the conditional PDF of the signal, according to the MLE principle. The estimated signal parameters (i.e. path delays, amplitude and phases) try to minimize the MSE of the LOS or multipath signal like:

$$s(t) = \sum_{l=1}^{L} \hat{\alpha}_l x(t - \hat{\tau}_l) e^{j(2\pi \hat{f}_d t + \hat{\Theta}_l)} \tag{4.13}$$

containing α_l, τ_l and Θ_l for the amplitude, delay and phase of the l-th signal, the estimated Doppler shift $\hat{f}_d$ and the time t. By setting such parameters to zero, equation 4.13 can be solved. The resulting equations can bee seen in [69], [70]. Whenever there is multipath, RSSML tries to separate the eventual incoming multipath signals from LOS components, by estimating all MLE signal parameters in consequence of the best curve fitting. To fulfill this, competitive peaks had been observed with a threshold, which is based on the estimated threshold and a weighting factor [66]. Next, the RSSML computes the MLE for each candidate delay index, so that one with a minimal error is chosen as the estimated LOS delay [70].

5 Level Crossing Rates

Usually widely used in mobile communications to optimize various parameters of the receiver, the LCR can be applied for fading channel or multipath. In order to determine statistical properties of the fading time intervals, the LCR can be used, which basically counts the crossings under a specific level [71]. In simulation, analytical expressions can be derived by Nakagami [72] or Rayleigh [73] processes.
As the major idea to detect multipath under NLOS scenarios, the LCR will be used. Therefore, this chapter provides general applications of the LCR and the use in NLOS detection.

5.1 General application of LCR

The LCR basically measures the rapidity of the fading. The result is to quantify how often the fading is crossing a specific threshold, which is defined by the level λ. Then it counts the crossing either from above or below, even in summary about such level. Whenever communication takes place, the wireless signal is interfered and power limited. Based on mathematical and physical analysis, the major idea is similar in several application fields. The received signal r and its derivative with respect to time $\dot{r}$ and the joint PDF function $p_{\dot{r},r}(\dot{r},r)$ are needed to define the average LCR in the closest form [74]:

$$\begin{aligned} N(\lambda_{th}) &= \int_0^\infty \dot{r} p_{r,\dot{r}}(\sqrt{\lambda_{th}},\dot{r}) d\dot{r} \\ N(r) &= \int_0^\infty \dot{r} p_{r,\dot{r}}(r,\dot{r}) d\dot{r} \end{aligned} \tag{5.1}$$

where N are the counted crossings, λ_{th} is the threshold of the LCR and r the received signal. The average of time, where the ratio remains below the threshold λ is determinate as the average LCR [75]:

$$T(r) = \frac{F(r)}{N(r)} \tag{5.2}$$

with $F(r)$ as the number of values under the threshold and $N(r)$, which is the

overall number of crossing. Such crossings can be used with $N(\lambda)$ as well. With respect to the previous mentioned basics, the following applications can be realized:

The **Outage Ratio** is the most commonly used performance measurement for radio communication systems [76] [77]. In the given case, the LCR is used to measure the right selection of the transmission symbol rate, interleave depth, packet length and time slot duration. If the Signal-to-Interference-Ratio (SIR) or received signal power falls below a certain threshold, that is λ or s_D, which is the threshold for the desired signal power crosses, an outage is declared [78]. The Average Outage Ratio (AOD) then describes the outage status in time with respect to equation 5.2:

$$T(\lambda_{th},s_{th}) = \frac{P_{out}}{N(\lambda_{th},s_{th})} \tag{5.3}$$

where the number of N crossing rates is defined by the SIR process crosses λ_{th}, or the desired signal power crosses s_{th}. The probability of the system outage is $P_{out} = P[\lambda < \lambda_{th} \text{ or } s_D < s_{th}]$ when there is a present minimum desired power restriction [79]. The AOD can be fully obtained by the LCR $N(\lambda_{th},s_{th})$. If the system is interference limited, λ is no part of the mentioned equations. Hence, the closest form for N is given by second equation in 5.1. For interference limited systems, N can be described as

$$N\left(\alpha_D = \sqrt{\lambda_{th}}\alpha_I | \alpha_I \geq \sqrt{\frac{s_{th}}{\lambda_{th}}}\right) = \int_0^\infty \dot{r} p_{r,\dot{r}|\alpha_I}(\sqrt{\lambda_{th}},\dot{r}) d\dot{r} \tag{5.4}$$

for a system with a minimum desired signal power constrained, with α_D and α_I as the composite amplitudes of the desired user and co-channel interferes. Afterwards, the received sampled envelope is $r = \alpha_D/\alpha_I = \sqrt{\lambda_{th}}$ and $p_{r,\dot{r}|\alpha_I}$, the conditional joint PDF [80] [81]. The Outage Ratio is described in detail in [78], [82] and [83].

A relatively new research for an effective method to mitigate multipath fading is **diversity combining**. Such method is about combining multiple received copies of the transmitted signal in the receiver. In [84], the most popular techniques are represented by the Maximal Ratio Combining (MRC) [85], Equal Gain Combining (EGC) [86] and Generalized Selection Combining (GSC) [87] at least.

The Rayleigh Channel Fading is most applicable under NLOS conditions. This channel is cascaded and can be modeled by the product of N fading amplitudes. In order to characterize this channel, a **Rayleigh channel characterization** can be done by use of the LCR. In wireless communication, multihop is providing a broader and more efficient coverage. It can be separated in either non-regenerative or regenerative [88] [89]. In such given case, the characterization, with respect to the underlying fading channel, can be done with help of the LCR [90]. As represented in [91] and [92], the evaluation is based on previous equation 5.2 as well.

5.2 CNR estimation

In fields of GNSS, the knowledge about the CNR can be important for positioning. A significant task is to assist various stages of the signal tracking for example. Besides to other estimators such as in [93], [94] and [95], the use of the LCR takes place in the Level Crossing Rate Estimation (LCRE) [96]. The non-coherent Cross Correlation Function (CCF) needs to be examined with respect to the number of downward and upward crossings with [97]:

$$LCR_{down}(\lambda) = \frac{1}{K_{tot}} card\left\{k|(z^{(k)} \leq \lambda) \text{ AND } (z^{k+1} \geq \lambda)\right\} \tag{5.5}$$

$$LCR_{up}(\lambda) = \frac{1}{K_{tot}} card\left\{k|(z^{(k)} \geq \lambda) \text{ AND } (z^{k+1} \leq \lambda)\right\} \tag{5.6}$$

where $K_{tot} = N_s N_{BOC} W$ as the total number of samples in the correlation window of W chips, an oversampling factor N_S and the BOC modulation order N_{BOC}. Furthermore, $z^{(k)}$ is the sample of the non-coherent CCF and λ is the threshold for the crossings. Here, the total number of the LCRs can be written as:

$$\begin{aligned} LCR_{total}^{(\lambda)} = \tfrac{1}{K_{tot}} \Big[\textstyle\sum_{k=\tau_{max}-N_S N_{BOC}}^{k=\tau_{max}+N_S N_{BOC}} LCR_{C1}^{(k)} + LCR_{C2}^{(k)} + ... \\ ... + LCR_{C3}^{(k)} + (K_{tot} - 2N_S N_{BOC} - 1) LCR_{C4}^{(k)} \Big] \end{aligned} \tag{5.7}$$

where C_i is defined by different situations (see table 5.1) with focus on the sample, $z^{(k)}$ and $z^{(k+1)}$, with the maximum peak at τ_{max}. A sample, which is located within one chip from the estimated code delay, calls Peak Point (PP), otherwise literature is talking about the Outside Peak Point (OPP). In [98], different cases were described as it is mentioned in the table 5.1. In there, ψ^2 denotes the chi-square distribution.

Table 5.1: LCR functions of the LCRE for all cases

Case	$z^{(k)}$	$z^{(k+1)}$	$LCR_C^{(k)}$
C_1	PP	PP	$LCR_{C1}^{(k)} = F_{\Psi^2\neq 0}^{(k)}(\lambda)\left(1 - F_{\Psi^2\neq 0}^{(k+1)}(\lambda)\right)$
C_2	OPP	PP	$LCR_{C2}^{(k)} = F_{\Psi^2= 0}^{(k)}(\lambda)\left(1 - F_{\Psi^2\neq 0}^{(k+1)}(\lambda)\right)$
C_3	PP	OPP	$LCR_{C3}^{(k)} = F_{\Psi^2\neq 0}^{(k)}(\lambda)\left(1 - F_{\Psi^2= 0}^{(k+1)}(\lambda)\right)$
C_4	OPP	OPP	$LCR_{C1}^{(k)} = F_{\Psi^2= 0}^{(k)}(\lambda)\left(1 - F_{\Psi^2= 0}^{(k+1)}(\lambda)\right)$

After the identification of all crossings had been done by equation 5.7, the CNR can be estimated by searching the maximum number of crossings with:

$$\widehat{CNR} = \arg\max\left(LCR_{total}^{(\lambda)}(CNR)\right) \tag{5.8}$$

5.3 LCR for NLOS detection

The major contribution of this master's thesis work is provided by using the LCR to detect multipath in NLOS situation. With respect to equation 5.5 and 5.6, the total number of crossings in the normalized correlation function $\overline{R}_k$ of k samples or chips at a threshold level λ is:

$$LCR(\lambda) = card\left\{k|(\overline{R}_k \leq \lambda \wedge \overline{R}_{k+1} > \lambda) \cup (\overline{R}_{k+1} \leq \lambda \wedge \overline{R}_k > \lambda)\right\} \tag{5.9}$$

with the cardinality *card* of a set and the union operator $\cup$. In the simulation results (see chapter 8), the issue of using the mean of the ACF for the crossing level λ will be mentioned (see section 7.2). Other possibilities are to use λ as the median of $\overline{R}_k$ function or as a fixed value. The empirical tests showed that using λ as the mean of the ACF in the considered window gives the best results (see section.

The CNR has to be estimated with, for example, the presented method in previous section 5.2, or based on some other approaches existing in literature, such as in [99] or [100], because the detection technique depends on it (see subsection 8.1.1). The tested algorithm can be formed as:

$$\begin{aligned}\gamma(x) &= f\left[\frac{1}{\sigma\sqrt{2\pi}}\exp\left\{-\frac{(x-\mu)^2}{2\sigma^2}\right\}\right] \\ &= f * \mathcal{N}(\mu,\sigma^2)\end{aligned} \tag{5.10}$$

A factor f is multiplied by a normal distribution, including the variance σ^2 and the mean μ with respect to the current CNR. The mentioned factors were estimated in the training phase and then evaluated in realistic conditions (see subsections 8.1.1 and 8.1.2). γ is representing the threshold in the decision of being in LOS or NLOS. Furthermore, x is containing the current number of crossings, which are counted by the level crossings at the level λ. During the simulation, the best approximation of the parameter have been done which will be mentioned in section 7.2.

Table 5.2: Decision of the presence of multipath in at the current mean level λ of the ACF and the CNR-based curve γ

Case	Threshold
Multipath	$\gamma > mean(\text{ACF}), mean(\text{ACF}) = \lambda$
One-path	$\gamma \leq mean(\text{ACF}), mean(\text{ACF}) = \lambda$

The decision if there is a presence of either multipath or one-path is done with the knowledge of the current ACF mean level λ and the output of the in previous calculated curve γ, representing the threshold. Such values are compared to identify the circumstances at hand. Mathematically, the measured ACF level λ is compared to equation 5.10 with respect of being located below or above, which can be seen in table 5.2.

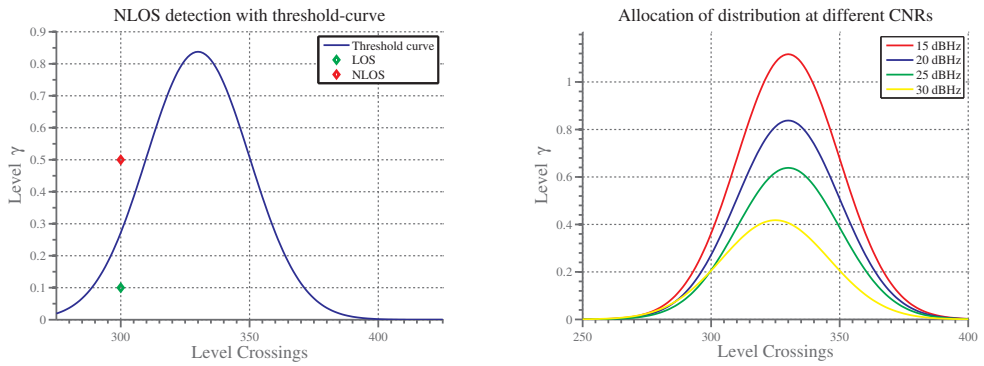

Figure 5.1: left: Decision of present multi- or one-path - red point: multipath, green point: one-path - right: Allocation of the threshold curve in different CNR environments

Referring to figure 5.1, the decision process can be observed for a simple example. While the red point is above the curve, which has been built with equation 5.10 under a certain CNR level, the green point is under the curve and is identified as a direct path, which means being in LOS.

In reality, the CNR is changing over the time. Even a moving receiver dues to varying circumstances. Hence, the normal distribution based technique must be calculated for every moment. The less strong the signal, the more crossings, caused by a higher dynamical curve shape, can be counted. This leads to an higher mean level of the ACF function and also a different use of parameters (see figure 5.1).

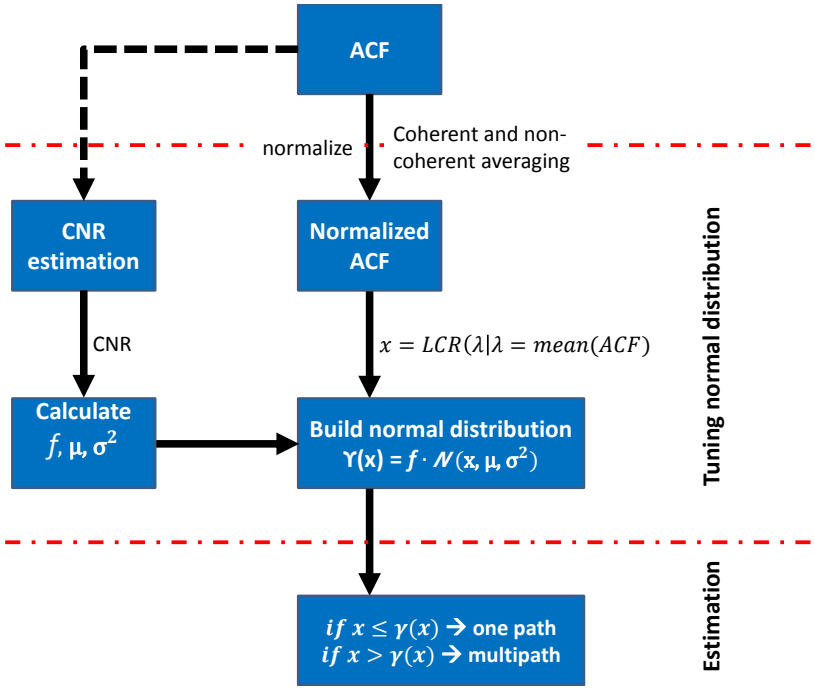

Figure 5.2: Block diagram of the NLOS detection based on a normal distribution

The presented NLOS detection can be seen in figure 5.2. In summary, following steps must be done:

1. The ACF can be used for the CNR estimation, which is necessary for step 4.
2. The coherent and non-coherent averaging must be done with the ACF. Afterwards, the ACF must be normalized.
3. The level crossings are counted by the mean of the normalized ACF ($x = LCR\,[\lambda|\lambda = mean(ACF)]$).

4. The parameters (f, μ, σ^2) of the normal distribution $\gamma(x)$ are calculated by the estimated CNR.

5. The number x of the crossings of the LCR at the level λ is compared to the normal distribution γ. If x is under the curve γ, a possible presence of one-path is detected. Otherwise, the presence of NLOS is estimated.

6 Simulation model

The investigation to detect the presence of multipath in NLOS scenarios had been done as described in this chapter. In general, the computation of the LCR was placed in different areas in the baseband process.

Because of using simulations to assess the results, the need of having the most realistic scenario for the Galileo signal is totally necessary to do an evaluation of the developed method. With respect to the performance, a signal had been produced by Matlab® (version R2013b), which is referenced in figure 6.1.

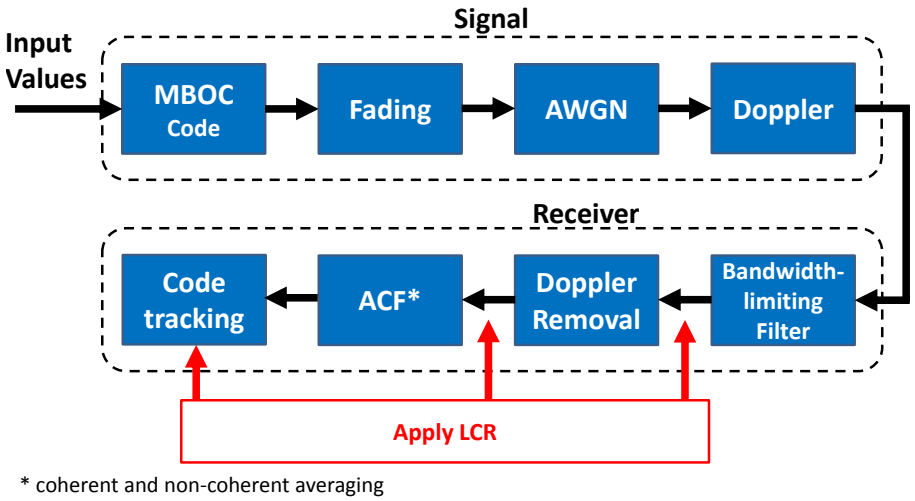

Figure 6.1: Block diagram of the used system

To ensure the dynamic nature of a signal, several values, such as the CNR, or the number of paths can be changed. A Multiplexed Binary Offset Carrier (MBOC) code is created by a weighted combination of SinBOC(1,1) and SinBOC (6,1). The certain factors were chosen for the Galileo used CBOC, as $w_1 = \sqrt{\frac{10}{11}}$ amd $w_2 = \sqrt{\frac{1}{11}}$. After oversampling, the code is passed through a fading (Rician, Rayleigh or Nakagami) and an additive white Gaussian noise (AWGN) channel. Afterwards, the Doppler shift is also added to the dataless code, so that the signal creation is complete. Next, at the receiver side (Matlab® implemented), the Doppler and the carrier frequency are removed and the signal is cross-correlated

with a stored CBOC-modulated replica. The chosen correlation window in the simulations was set to 50 chips, because the introduced maximum channel delay was set to 10 multiplied with the number of paths. The LCR was applied in three different situation in the baseband processing on the

1. filtered signal after the bandwidth limitation,
2. filtered signal after the bandwidth limitation and Doppler removal and
3. Auto-Correlation-Function, meaning post-correlation.

The chosen simulation parameters can be observed in table 6.1.

Table 6.1: Simulation parameters, which were used in the simulations

Parameter	Symbol	Value	Unit
CBOC weighting factors	$w_{1,2}$	$\sqrt{\frac{10}{11}}, \sqrt{\frac{1}{11}}$	$[-]$
Chip frequency	f_c	1.023	MHz
Coherent integration length	N_c	4	$[-]$
Correlation window	$[-]$	50	Chips
Maximum multipath separation	x_{max}	0.35	Chips
Minimum multipath separation	x_{min}	0.02	Chips
Non-coherent integration length	N_{nc}	1	$[-]$
Receiver bandwitdth	B_T	[4:4:16]	MHz
Spreading factor	S_F	1023	Chips

The detection part takes place in the baseband process of the receiver. The three stages of applying the LCR contain a different progress of the signal. The filtered signal and the removed Doppler shift looks quite similar as it can be seen in figure 6.2. The two cases of the ACF after the Doppler removal with and without averaging can be seen figure 6.3. Once the signal is compared to the replica inside the storage of the receiver, the correlation can be done. Afterwards, the ACF can be averaged with the coherent and the non-coherent integration. The LCR, which is applied on the ACF, makes use of the correlation after the non-coherent integration, which is first normalized.

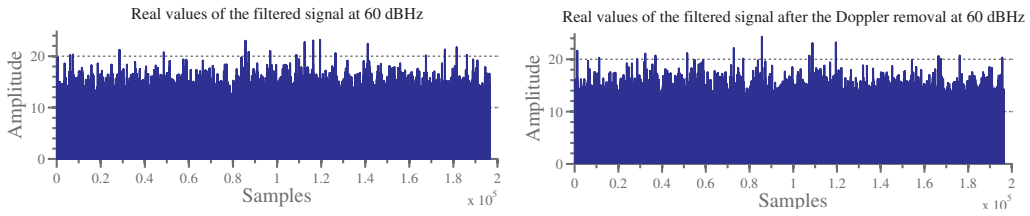

Figure 6.2: Filtered signal before and after Doppler removal for two-path signal

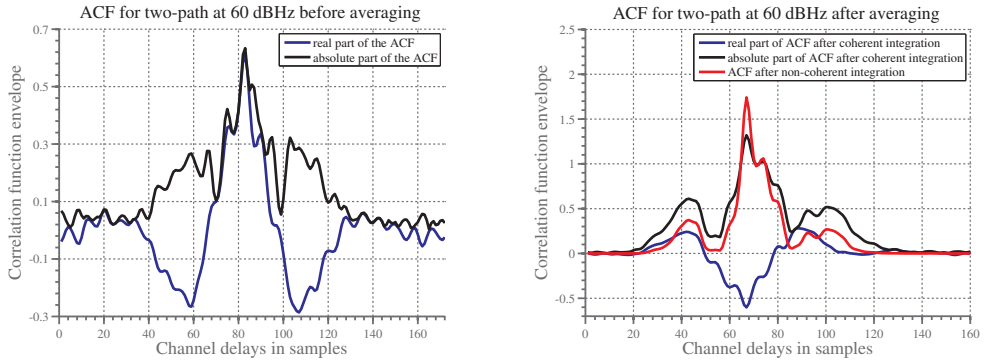

Figure 6.3: ACF of the filtered signal with and without averaging after the Doppler removal for a two-path signal

7 General LCR application

This chapter is dealing with the implementation of the LCR to detect multipath and with the idea of differentiating several scenarios under NLOS or LOS, which was presented in section 5.3. First, the level crossings were applied in three different stages as in figure 6.1 and explained in chapter 6. The best allocation was to apply the LCR at the output of the correlation with the replica code, which was tested with several channel fading types and several configurations. In here, the training phase contains the basic implementation of the level crossings, respectively the normal distribution based algorithm and an additional possibility to increase the average detection percentage.

7.1 Introduction of LCR implementation

First, the LCR was applied in three receiver stages (chapter 6). In particular, this test was done in one-path and multipath between two and three paths in order to find some rules of detection. The CNR level was varying within a large window to include every scenario by choosing the range of [20:20:60] dBHz and 500 loops per path. The idea of having a level for a decision, if there is a presence of multipath, was done by a probability of the crossings, plotted over the LCR threshold level λ. λ has been also fine-tuned empirically, first taken as various fixed values, then by using mean or median of the ACF over a certain window, and lastly by employing statistical fit to the data as explained later in this chapter.

Referring to figure 7.1, 7.2 and 7.3, the PDF of the LCR under one-, two- and three-paths, respectively and for three CNR levels (good and moderate CNR in the upper plots and low CNR in the lower plot) can be seen. When the LCR is applied after the bandwidth-limiting filter of the receiver (see figure 7.1), the observable curve shows, that it is difficult in here to find a rule for the multipath detection under NLOS. While the amounts of one-path crossings are below those of multipath in a good CNR scenario, here 60 dBHz, in other situations such as 40 dBHz, the amount of crossings are above. The level crossing rates are neither always higher in single path than in multipath, nor smaller, but they fluctuate

without a clear rule. This is expected since the noise level in the pre-correlation domain is very high. Hence, the detection of multipath is not suitable in this approach (LCR at pre-correlation and pre Doppler removal level) because of having random conditions.

Next, the LCR was applied after the bandwidth-limiting filter and after the Doppler had been removed (figure 7.2). As a result, by using the previous parameters, the level crossings are following nearly the same process as before. In good CNR conditions, multipath can be clearly separated. In cases of a high CNR, a differentiation might be not successful. By mentioning the example of a signal from 20 and 40 dBHz, the probability of LOS at its best is located under multipath. However, a better signal indicates a fluctuation of the LCR probability that is not suitable for the NLOS detection.

The LCR results of the bandwidth-limited filtered signal show a difficult situation in terms of detection. Because of that, the next step was to apply the LCR at the output of the normalized non-coherent ACF. The plots in figure 7.3 show stable properties of the direct path crossings in comparison to those of the filtered signal. The PDF of the LOS scenarios are separated from affected signals. The better the CNR is, the less crossings are measured, because the ACF shape is not oscillating highly. According to these issues, the thesis based on the LCR applied at the ACF level, i.e., after the correlation and coherent and non-coherent averaging.

The impact of the presence of multipath in the ACF can be seen in figure 7.4. By extracting the normalized ACF after the averaging, the curve shape of both curves are different. In LOS situations, the channel delay is equal to zero, the ACF is nearly symmetrical and the main peak has only one maxima. If the signal passed more paths, such as three in this example, the curve is asymmetric. The main peak does contain two maxima, the width of such peak is bigger than by having a direct path. Because the signal is more disturbed in situations of multipath, the threshold level λ, which is set as the mean for the level crossings, is higher with $\lambda = 0.0113$ than the threshold level for one-path with $\lambda = 0.0061$.

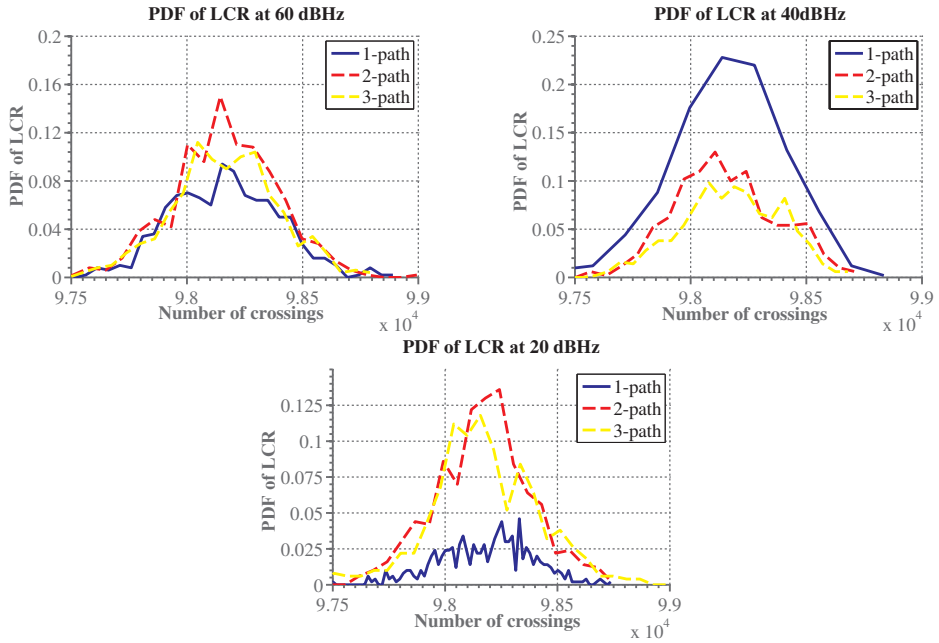

Figure 7.1: Applied LCR after the receiver filter - Level λ of LCR = mean(ACF), Number of measurements per path = 500

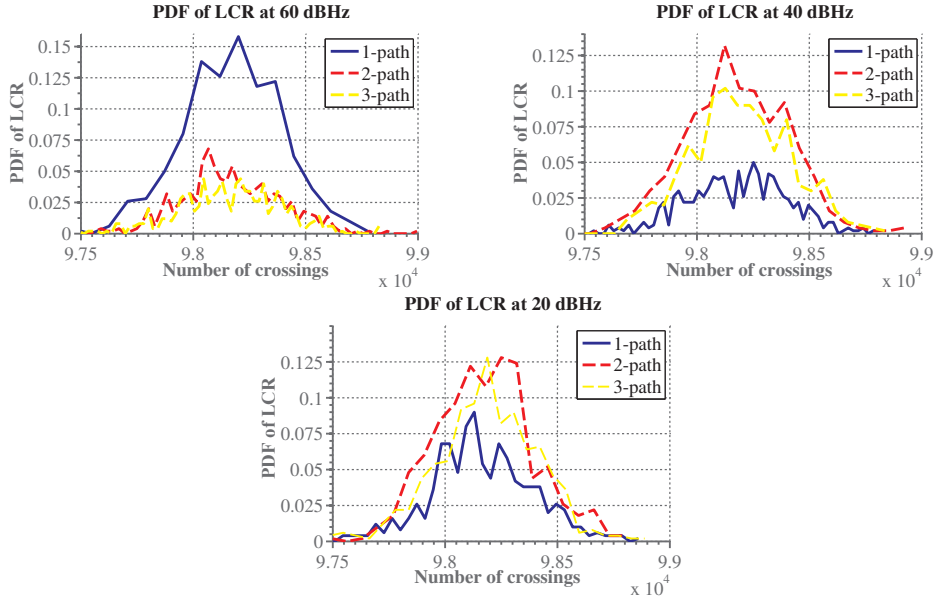

Figure 7.2: Applied LCR after the bandwidth-limiting receiver filter and after the Doppler removal, but before correlation - Level λ of LCR = mean(ACF), Number of measurements per path = 500

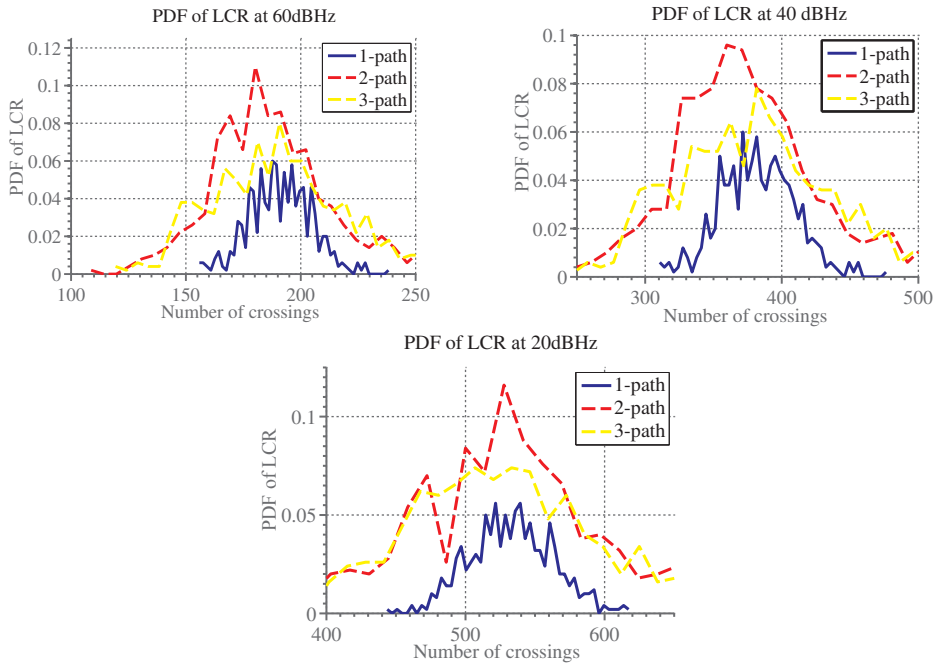

Figure 7.3: Applied LCR on the non-coherent Auto-Correlation Function, after the correlation and averaging - Level λ of LCR = mean(ACF), Number of measurements per path = 500

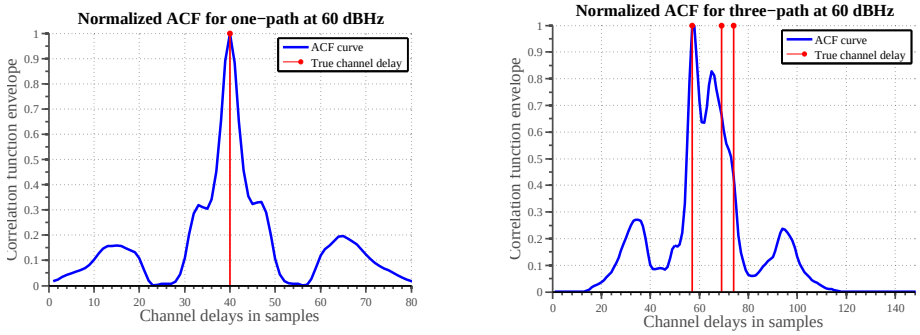

Figure 7.4: Normalized ACF at 60 dBHz for one and three path with true channel delays. Left: LCR level λ = 0.0061 - Right: LCR level λ = 0.0113

7.2 Normal distribution based algorithm

In section 5.3, the basic idea of using the LCR to detect NLOS, respectively multipath, was presented. The threshold-curve γ, which is calculated by equation 5.10, can be evaluated by an average detection percentage that is:

$$E[\%] = \frac{100 - p_1 + \sum_{n=2}^{n}(p_n)}{n+1} \tag{7.1}$$

where p_1 and p_n are the detected multipath situations of one- and the n^{th} multipath in percentages [%] of the detected multipath situations. If there is a single path, the correct detection percentage is 100-p_1, because p_1 measures the percentage of points in which the multipath is detected. By having this average detection percentage, the success of correctly detected situations, either LOS or NLOS, can be evaluated and compared. The equation needs to be adjusted for either having one- or multipath. In LOS situations, p_1 needs to be subtracted and p_n added, because p_n describes the detection percentages of multipath.

First, the LCR was basically tested for three fading channel types including Rician, Rayleigh and Nakagami channel with the previously mentioned average detection percentage. The CNR was used in the interval [20:20:60] dBHz and the input parameters of the normal distribution γ (equation 5.10) was chosen by an adequate range (table 7.1). The results are based on having 500 generated signals for every path in every CNR case.

Table 7.1: Parameter range (f,μ,σ) of the normal distribution-based algorithm to evaluate different fading channels

Parameter	Symbol	Range of the values
Sigma	σ	[1:0.25:70]
Mu	μ	[1:0.25:400]
Multiplier	f	[1:0.25:80]

The Rayleigh fading channel achieves the best results in comparison to the Rician or Nakagami (see table 7.2) with respect to the average detection percentage for a known CNR case. In lower CNR environments, the detection of correct paths is higher for Nakagami than for Rayleigh and Rician. But the Rayleigh fading channel shows the best results with the developed detection technique in overall. Hence, this channel was chosen for all following parts of this thesis. The Rayleigh fading channel provides good simulations for NLOS as mentioned in

[101].

Table 7.2: Average detection percentage for different fading channel types between one- and three-path

Fading Channel Type	CNR [dBHz]	p_1^*[%]	p_2[%]	p_3[%]	Average Detection Percentage [%], as in eq. 7.1
Nakagami	20	28.4	63.2	67.6	67.4
	40	16.0	55.6	63.0	69.8
	60	1.0	86.8	84.0	92.9
Rayleigh	20	10.2	59	61.1	74.4
	40	18.8	79.2	89.6	80.2
	60	0.8	95.0	97.8	97.1
Rician	20	6.8	41.6	44.4	67.4
	40	9.4	53.6	56.2	72.1
	60	12.6	65.4	71.0	76.4

Statistically (in 95% out of 13.500 measurements), the detection of multipath in three-path scenarios is better than in situations of two-path, as it can be seen in table 7.2. Therefore, the higher the number of multipaths, the better the separation between NLOS and LOS can be done in most cases.

In table 7.2, the average detection percentage based on the results between single- and the certain multipath, e.g (100 - p_1 + p_3)/2. As previously described, the detection of one-path (p_1^*) is done by 100-p_1^*, because p_1^* contains the detected multipaths in percentages. Therefore, the results of the detected multipaths in a one-path case needs to be subtracted.

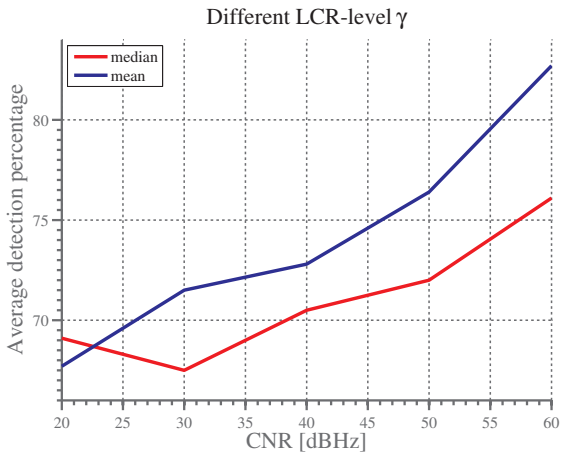

Figure 7.5: Average detection percentage with mean and median level for γ - Random points: 500 per CNR - Fading channel: Rayleigh. Known CNR case.

As previously mentioned, the NLOS detection technique makes us of the mean level, which is based on the correlation function. This threshold level λ is then compared to a certain normal distribution based curve γ with respect to the current CNR. The most reliable multipath detection can be done with the mean of the level λ of the normalized correlation. By comparing the results in dependence of λ, referring to figure 7.5, the average detection percentage is high for the mean so that the crossings should be counted as $x = LCR\,[\lambda|\lambda = mean(ACF)]$.

7.3 Improvement of LCR

By having a closer look to some improvements, the idea of allowing only crossings with a bigger distance between two local maxima can be justified in following. The successful detection of different multipaths can be increased, while reducing the error of wrongly detected direct paths as multipath. When the LCR is done, the output, besides to the threshold level λ and the number of crossings x, is the location on the x-axes (in samples or chips) and the y-axes (coherent function envelope) of such crossings in the ACF.

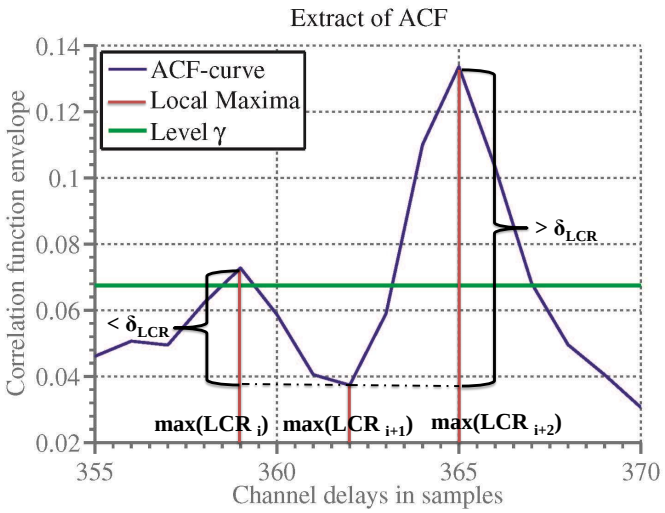

Figure 7.6: Illustration of the improved detection by an extract of the ACF with level γ. While max(LCR_i) and max(LCR_{i+1}) are under the threshold δ_{LCR}, max(LCR_{i+1}) and max(LCR_{i+2}) are over it. - Rayleigh channel - CNR = 40dBHz

If now the positions of the crossings are known, an implemented algorithm can search for local maxima between two crossings, which is the searching range for a local maximum or minimum (see figure 7.6). When all local maxima are allocated, the distance between two local extrema should be over a threshold δ_{LCR} to be considered:

$$|max(LCR_i) - max(LCR_{i+1})| > \delta_{LCR} \ \vee \ |max(LCR_{i-1}) - max(LCR_i)| > \delta_{LCR} \quad (7.2)$$

where $max(LCR_i)$ is the i^{th} maximum or minimum between two crossings. Hence, the number of LCR decreases, but the results are better which can be seen in table 7.3.

Table 7.3: Average of the improved average detection percentage between one- and three-path

	1-path	2-path	3-path
Average of improved average detection percentage [%]	4.22	5.96	5.45

The results of using the previously mentioned improvement can be seen in figure 7.7. According to the curves, the average detection percentage can be increased. In all CNR cases within the range of 20 to 40 dBHz, the average of the improvement of the detection percentage is better in multipath than in one-path cases (see table 7.3).

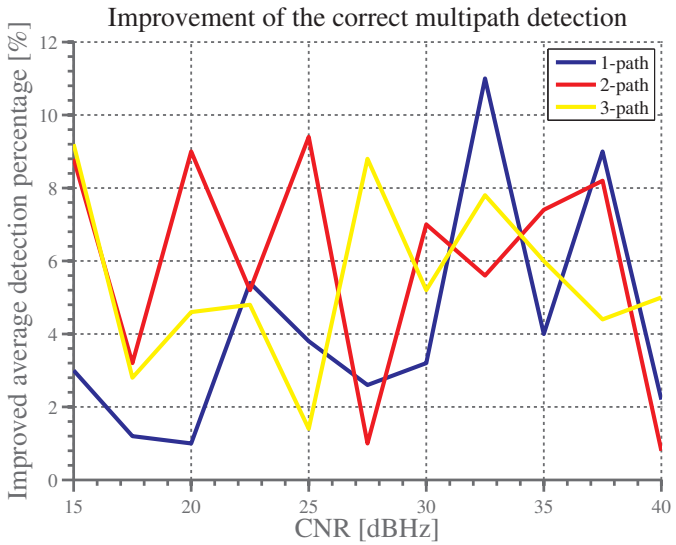

Figure 7.7: Improved average detection percentage in overall by having the ideal estimated CNRs

8 Simulation results

This chapter presents the simulation results, including performance tests , the fixing of the parameters (f, μ, σ) and a benchmark test. The developed model was tested in several realistic situation to ensure the reliability.

8.1 Performance of multipath detection

This section represent the major interest about the thesis. In here, the performance test and the fixing of the parameters will be done and evaluated. With respect to section 5.3, where the algorithm was introduced, and basically section 7.3, in which the improvement was described, the NLOS detection technique can be evaluated. To produce reliable results, this chapter was produced by covering the CNR for NLOS cases by [15:2.5:40] dBHz. To create an average, which is used for the evaluation, 500 random correlation functions were produced in every of up to four paths and for every signal strength. A sampling rate N_S = 4, a non-coherent integration length N_{nc} = 1 block and a coherent integration length N_c = 4, were implemented in the signal creation. The receiver bandwidth was set to 16 MHz.

8.1.1 Fixing parameters

In order to modify the parameters f, μ and σ, used by the normal distribution based algorithm γ (equation 5.10), the search window were chosen by the threshold δ_{LCR} = [0:0.02:0.5], sigma (σ) = [1:0.25:70], mu (μ)= [100:5:400] and the multiplier (f) = [1:0.25:80]. These parameters need to be approximated in certain cases with respect to the CNR, as it has been described in figure 5.2 within the section 5.3.

The tests in before had been basically done by cover a huge range of the parameters. As it is presented in figure 8.1, the best results had been produced by the ideal curves. The allocation of the parameters inside the graph is rapidly switching sometimes, when the signal strength increases. A chart, that was sorted with

the criteria of the average detection percentage, was created in the calibration phase, based on the optimization process of choosing f, σ and μ parameters. The curves of the parameters were tuned as it can be seen in figure 8.1, represented by the "fitted" curves. Such curves were set with respect to the average detection percentage and a reproducible curve shape, which has to be approximated with the estimated CNR (see figure 5.2).

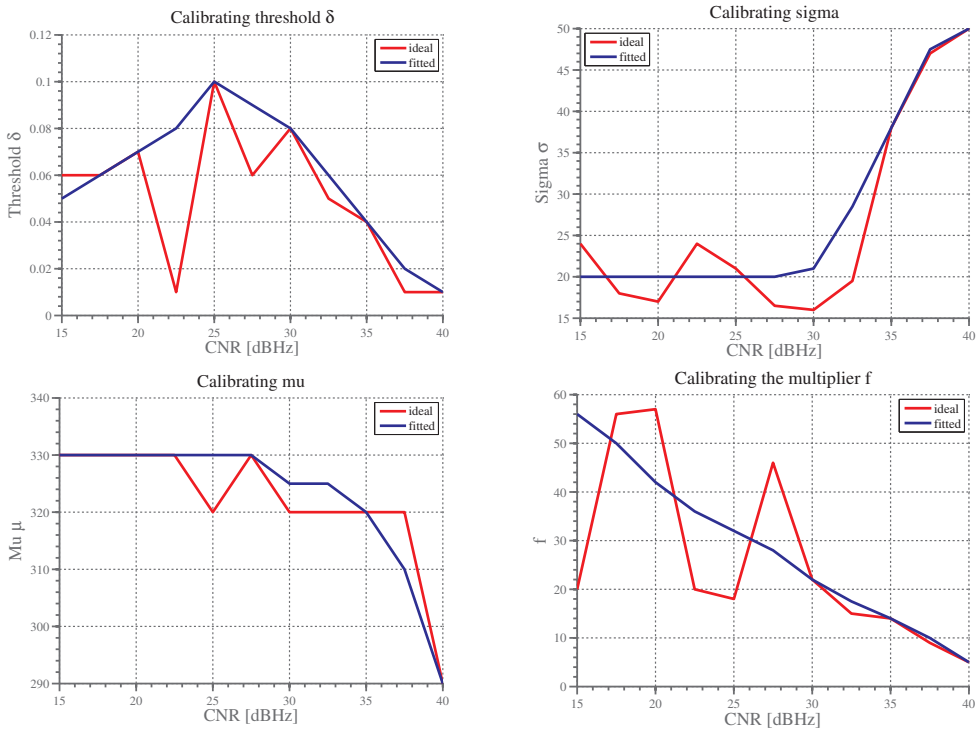

Figure 8.1: Adjustment of the parameters f, μ and σ for the normal distribution based algorithm (equation 5.10). The "fitted" parameters had been chosen with respect to the average detection percentage and a reproducible curve shape by an approximation.

By using more than one approximation for each parameter curve shape, which better fits the run of the curves than one approximation, it ensures the best accuracy in detecting multipath correctly. Based on the observations, which had been done with figure 8.1, the location of each factor was approximated by a polynomial of the n^{th} degree. The chosen polynomial, produced by diversifying the parameters f, μ and σ, can be seen in table 8.1. A reduction of the grade n was considered, such tested approximations ensure reliable results in identify NLOS at the same time.

The results of now using the approximated curves (table 8.1) are represented in figure 8.2 in comparison to the ideal run of the curve by using the ideal factors (see figure 8.1). Even a calculation of the approximated parameters can be done

Table 8.1: The approximation which ensures the highest amount of correct detection.

Factor	CNR-window [dBHz]	Approximation
Threshold (δ_{LCR})	15-25	$2.286 * 10^{-4} * CNR^2 - 4.343 * 10^{-3} * CNR + 6.457 * 10^{-2}$
	25-32.5	$-1.067 * 10^{-4} * CNR^3 + 8.8 * 10^{-3} * CNR^2 - 2.453 * 10^{-1} * CNR + 2.4$
	32.5-40	$4 * 10^{-4} * CNR^2 - 3.58 * 10^{-2} * CNR + 8.015 * 10^{-1}$
Sigma (σ)	15-27.5	20
	27.5-32.5	$5.2 * 10^{-1} * CNR^2 - 29.50 * CNR + 4.38 * 10^2$
	32.5-40	$-2.8 * 10^{-1} * CNR^2 + 23.26 * CNR - 4.32 * 10^2$
Mu (μ)	15-27.5	330
	27.5-32.5	$-4.444 * 10^{-2} * CNR^3 + 4.171 * CNR^2 - 1.312 * 10^2 * CNR + 1.706 * 10^3$
	32.5-40	$-4.444 * 10^{-2} * CNR_dBHz^3 + 4.171 * CNR^2 - 1.312 * 10^2 * CNR + 1.706 * 10^3$
Multiplier (f)	15-32.5	$3.476 * 10^{-2} * CNR^2 - 3.82 * CNR + 1.054 * 10^2$
	32.5-40	$-6 * 10^{-2} * CNR^2 + 2.69 * CNR - 6.575$

by ensuring a high average detection percentage at the same time. Except at 32.5 dBHz, where the detection percentage measured by the approximation, is 11.4 % below the ideal one and a similar curve from 35 dBHz up to 40 dBHz. The degradation, with respect to the successfully detected multipaths, of using fitted curves is quiet small.

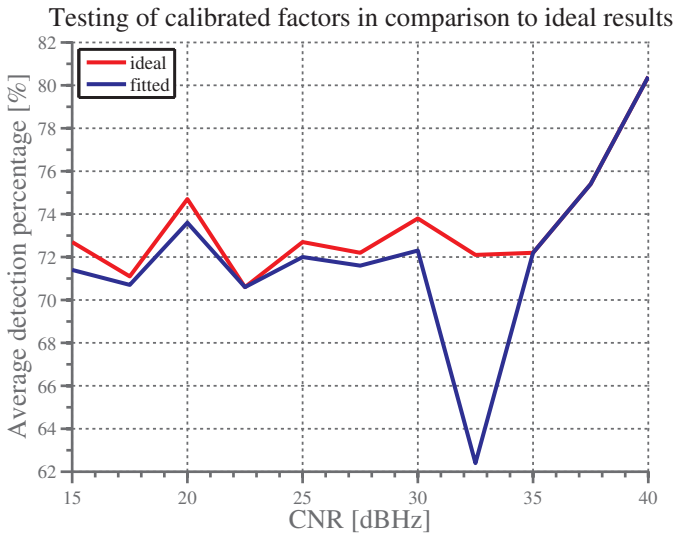

Figure 8.2: Average detection percentage of the ideal and "fitted" parameters

8.1.2 Performance tests

Now, applying the LCR and the modified threshold curve with the task to detect multipath in NLOS conditions, this part is presenting the performance tests of the developed multipath detection technique. Basically, this detection had been performed in typical NLOS circumstances between 15 and 40 dBHz.

The normal distribution based algorithm measures the threshold level λ of normalized ACF over the number of crossings x of the LCR (see figure 5.1). In the case of little disturbances and less delay in multipath, the detection of two-path is awkward in comparison to a higher amount of multipaths. This is due to the fact, that the allocation of two-path crossings are close allocated to the crossings of one-path. Moreover, the allocations of one-path crossings are less concentrated in lower CNR environments. Referring to figure 8.3, the success to identify one-path correctly is higher rated than the success in multipath. As stronger the signal, as better the average detection percentage in detecting correctly, except direct paths. By having a LOS with a higher CNR, the detection of multipath is increasing with respect to the percentage, while it is decreasing for one-path.

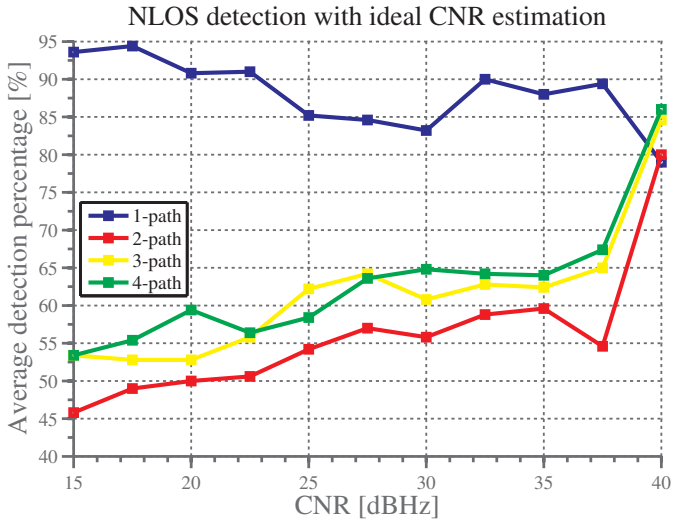

Figure 8.3: Results of performing the NLOS detection with ideal CNR estimation

In having a closer look to different receiver bandwidths-limiting, the performance had been tested as well. Referring to figure 8.4, the detection is relatively stable by changing the bandwidth-limiting of the receiver. In lower CNR scenarios, when having a lower bandwidth, the average detection percentage is oscillating more than in using higher bandwidths. In general, the detection is not depending on the bandwidth. Nevertheless, higher bandwidths are recommend because of the nearly linear average percentage detection.

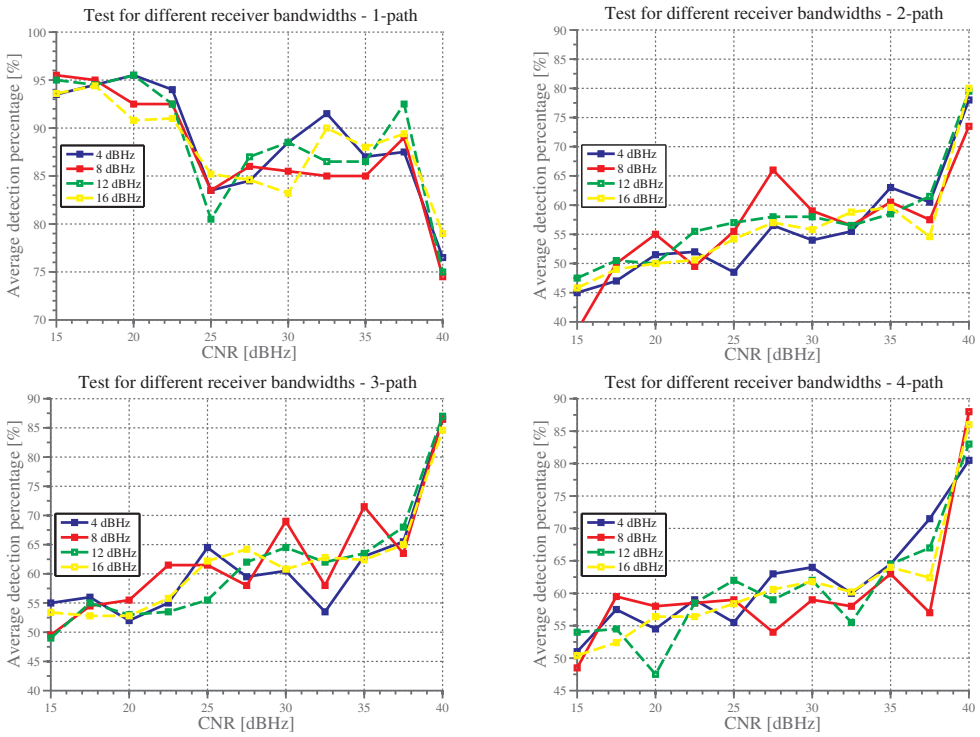

Figure 8.4: Testing of NLOS detection with different receiver bandwidths-limiting from 4 dBHz to 16 dBHz and ideal estimated CNRs

So far, the NLOS detection technique was tested by having an ideal CNR estimation. But in reality, the estimation of such value contains an error. The importance of the CNR had been figured out before, because the approximations of the parameters f, μ and σ for the normal distribution γ is done after the CNR estimation (see figure 5.2). The developed algorithm has been tested with two Carrier-to-Noise-Ratio estimators, one based on the LCR presented in section 5.2 and one estimator based on first order moments. In [100], the moment based CNR estimator was presented. Such estimator considers the correlation with the incoming signal and the stored reference code.

The developed NLOS detection technique highly depends on the CNR estimation. Referring to figure 8.5, the average detection percentage decreases by having an error in the CNR estimation. The moment based implementation is accurate in high CNR environments, but less high by having a small signal strength with respect to the Root Mean Square (RMS) (see figure 8.6). Such used estimator decreases the average detection percentage as it can be seen in figure 8.5 or table 8.2.

The average detection percentage is better for the LCR-based CNR estimator in multipath cases, but very bad for single path in higher CNR environments (see figure 8.5). By observing the RMS of the level crossing rate-based estimator in figure 8.6, the error is constant, but high in overall. An accurate estimation of the CNR in high CNR cases is necessary for one-path, because the average detection percentage is not suitable over 30 dBHz. In overall and according to table 8.2, the performance of the normal distribution based NLOS detection is the worst in comparison to the ideal or moment based CNR estimator.

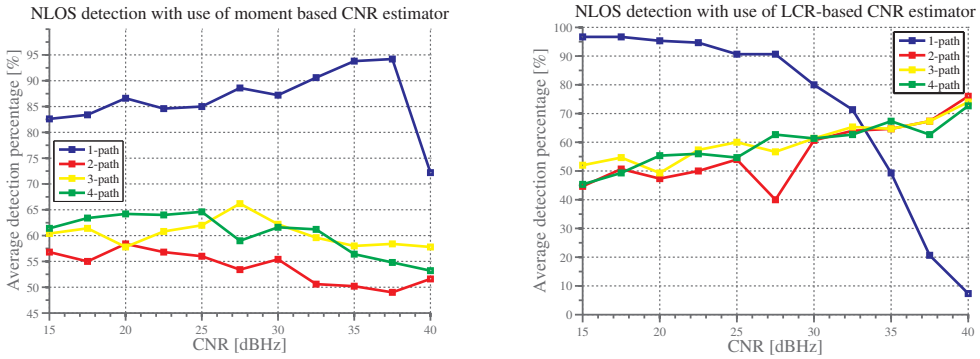

Figure 8.5: Results of performing the NLOS detection with different CNR estimators - left: Moment based CNR estimators for BOC/BPSK modulated signal for Galileo/GPS [100] - right: Level crossing rate- based estimation [98]

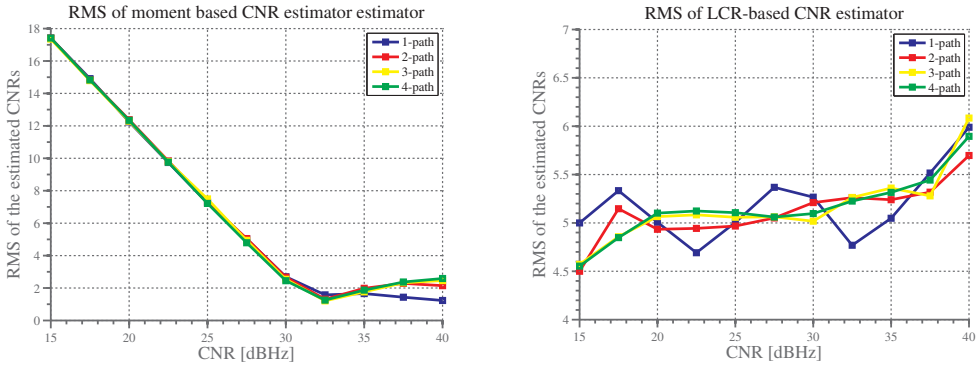

Figure 8.6: RMS of the used CNR estimators for single and mulitpath cases by 500 random points . left: moment based CNR estimator - right: LCR-based CNR estimator

Table 8.2: Average detection percentage [%] in average for all paths and different CNR estimators based on 500 measurements per path and CNR

	1-path	2-path	3-path	4-path
ideal CNR	88.11	55.95	61.53	61.44
moment based CNR	86.25	53.93	60.42	60.54
LCR-based CNR	77.12	56.30	60.24	59.09

8.2 Benchmark test

In literature, there are no common existing NLOS detection techniques, which are based on the ACF. Therefore, a simple method had been chosen to evaluate the normal distribution based algorithm. Basically, the benchmark measures the width of the main peak of the ACF and then compares this value with a calculated ideal one, based on no multipath.

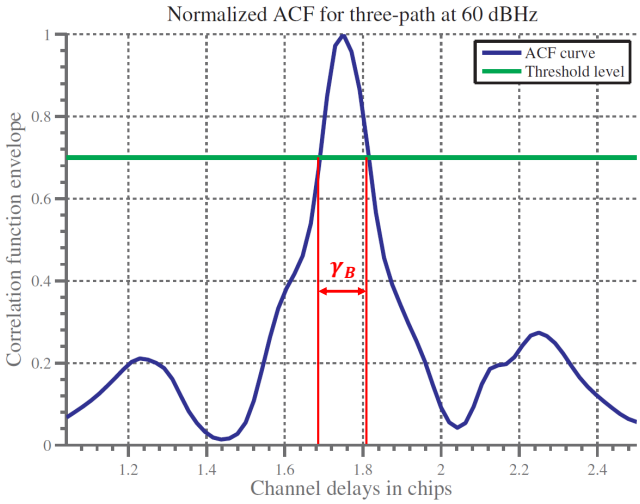

Figure 8.7: Principle of benchmark used for NLOS detection

Referring to figure 8.7, the benchmark takes the main peak of the normalized ACF. By adding a threshold level λ_b at 0.7 in the simulations, the distance or width between the crossings of the main peak can be measured in chips. Then, the ideal width, respectively γ_b, is calculated. Therefore the position of the maximum peak has to be figured out in the beginning. The threshold γ_b is set by all values of the ACF, which are above the threshold level λ_b in the search range:

$$n_{start} = \left[x_{max(ACF)} - N_s N_{BOC}\right]; n_{end} = \left[x_{max(ACF)} + N_s N_{BOC}\right] \tag{8.1}$$

where n_{start}/n_{end} is the start and end of the search range, $x_{max(ACF)}$ is the position of the maximum of the ACF in samples, N_s as the sampling factor and N_{BOC}, which represents the BOC-modulation order, here the maximum delay. Once the samples over the threshold level λ_b have been counted within this previously mentioned range, this amount represents the ideal width, respectively the decision threshold γ_b, either in samples or chips. At least, the width of the ACF at the level λ_b is compared to the decision threshold γ_b with the decision in table 8.3.

Table 8.3: Decision of having NLOS of the benchmark test (in chips) by comparing $width(ACF_\lambda)$ (width of peak at threshold level λ_b plus $\epsilon = 1 * 10^{-6}$ (error) with the measured threshold width γ_b

Case	Threshold
Multipath	$\gamma > width(ACF_\lambda) + \epsilon$
One-path	$\gamma \leq width(ACF_\lambda) + \epsilon$

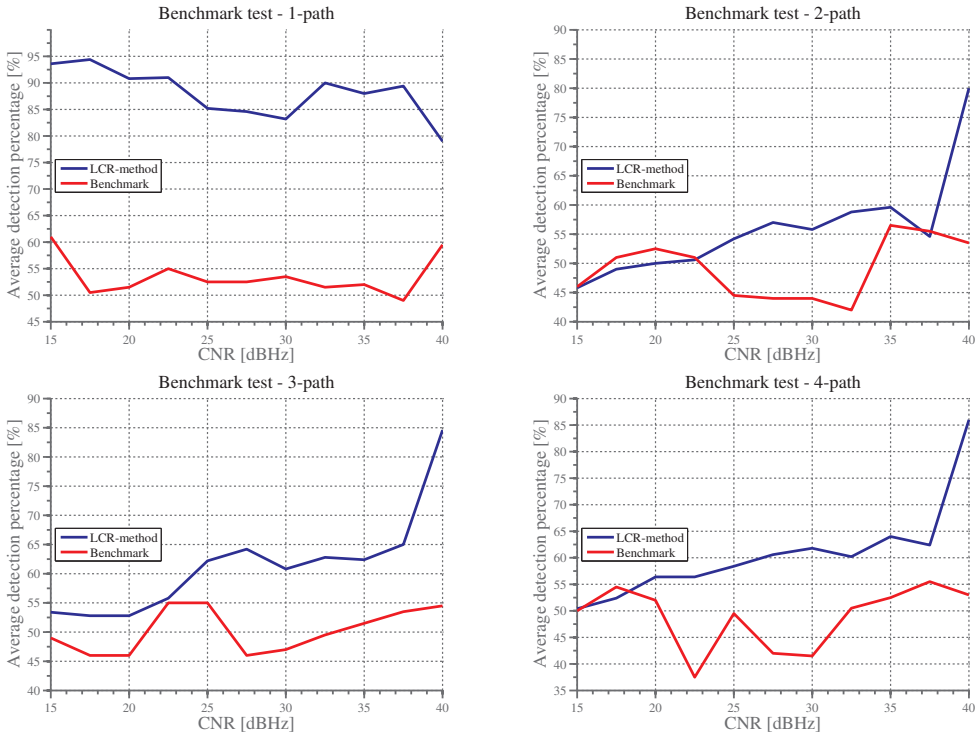

Figure 8.8: Comparison of the NLOS detection technique and a benchmark between one- and four-path for typical NLOS environments by having an ideal CNR estimation.

The correct detection of one-path is done much better with the crossing rates than with the benchmark test, referring to figure 8.8. In having lower CNRs the

successrate of the multipath detection is nearly similar for both tests. The average detection percentage is caused by the previously mentioned one-path detection higher for using the developed LCR technique than the benchmark. If the signal is increased, the average detection percentage of the LCR technique is increasing, where the benchmark test stays at the same level.

9 Conclusions and open discussion

The detection of multipath in NLOS scenarios is a complex field in positioning, as it had been addressed in this master's thesis. The detection had been successfully done within the ACF by using the LCR.

In this thesis, the level crossings were applied on the non-coherent ACF with suitable results. Besides such allocation of the LCR, a multipath detection has been done at sample level. At such stage, after the bandwidth-limiting filter and such filtered signal after the Doppler removal, the results were not promising (see section 7.1). Hence, the major implementation of the LCR has been done on the ACF after the non-coherent averaging and normalization.

The proposed technique had been designed for the CBOC signal under various parameters to simulate a realistic environment (see chapter 6). The developed NLOS detection technique was working properly in 70 % of all studied cases. While one-path and multipath can be successfully detected for up to 93.4 % for strong signals and up to 50.4 % for weak signals, the multipath detection is promising a higher average detection percentage for a better signal strength, quantitatively over 80 % in detecting multipath.

By using a normal distribution based algorithm (see section 7.2), several factors had been figured out and fixed (see subsection 8.1.1). The algorithm itself is stable in terms of changing the parameters. As in comparison to use ideal parameters, that had been searched first, the "fitted" ones are performing nearly similar, even in high CNR environments, which points out towards the fact, that the parameter optimization process worked very well.

Regarding the simulations, lower CNRs are leading to a worse separation between one- and multipath cases. As a result, the detection of a non-direct signal is much more difficult than at higher CNRs. On the other hand, a better signal includes a better multipath detection and a worse correct one-path detection at the same time (see subsection 8.1.2).

As it was mentioned in the simulations, the bandwitdth-limiting of the receiver does not have a big influence in the detection of NLOS. But higher receiver bandwidths-limits are recommended, so that an oscillation of the average

detection percentage can be prevented in results (see subsection 8.1.2).

With respect to the benchmark, presented in section 8.2, the found technique is much more promising and an indicator for a productive future research. It performed significantly higher compared to the benchmark. Especially the correct one-path detection does perform enormously better for the developed NLOS detection technique.

The limitation of this technique mainly is about the oversampling rate and the fixed ACF window of 50 chips, which must be chosen. Otherwise, the crossings are increasing and shifting the mean λ of the level crossings to a higher amount, that results in a worse average probability detection, if the parameter are not adjusted. Hence, an improvement needs to be done in the future.

Moreover, the normal distribution based detection technique highly depends on an accurate CNR estimation. Because of the used parameters f, μ and σ, which are calculated by the current CNR (see subsection 8.1.1), a good estimation is totally necessary. Otherwise, the correct detection of the current circumstances are worse (see section 8.1). It was shown, that the moment based CNR estimator results in a better average detection percentage for the NLOS detection in single path than the LCR-based technique. But the NLOS detection in multipath cases is higher for such LCR-based CNR estimator.

The LCR might be useful for multipath detection in NLOS. The difficulty of having a non-direct path is a major problem in this case. An optimization of the design parameters could be done. However, the preliminary tests on the LCR on the pre-correlation ACF were not showing promising results in this thesis. It is also of interest to find other multipath detection techniques in NLOS situations and to compare them with the LCR-based multipath detection.

Bibliography

[1] W. Rahiman and Z. Zainal. An overview of development GPS navigation for autonomous car. In *2013 8th IEEE Conference on Industrial Electronics and Applications (ICIEA)*, pages 1112–1118, Melbourne, Australia, June 2013. IEEE.

[2] W. Mansfeld. *Satellitenortung und Navigation. Grundlagen, Wirkungsweisen und Anwendung globaler Satellitennavigationssysteme*. Springer, third edition, 2010.

[3] P. J. G. Teunissen and A. Kleusberg. *GPS observation equations and positioning concepts*, volume 60 of *Lecture Notes in Earth Sciences*. Springer, 1996.

[4] *GPS Basics: Einführung in die GPS Vermessung (Global Positioning System).* Leica Geosystems AG, first edition, 2010.

[5] M. Sawabe S. Kogure, M. Kishimoto and K. Terada. Performance Analysis of the QZSS SIS-URE and user Positioning Accuracy with GPS and QZSS. In *Proceedings of the 2008 National Technical Meeting of The Institute of Navigation*, pages 452–457, San Diego, USA, January 2008. ION.

[6] U.S. Departement of Homeland Security. GPS CONSTELLATION STATUS FOR 05/12/2014. http://www.navcen.uscg.gov/?Do=constellationStatus, opened on 12/05/2014.

[7] E. D. Kapplan and C. Hegarty. *Understanding GPS: Principles and Applications, Second Edition*. Artech House; second edition, 2005.

[8] B. Hofmann-Wellenhoff, H. Lichtenegger, and E. Wasle. *GNSS - Global Navigation Satellite Systems: GPS, GLONASS, Galileo, and more*. Springer Vienna, 2008.

[9] European GNSS (Galileo) Open Service, 2010. Galileo OS ICD, issue 1.1.

[10] B. Bhatta. *Global Navigation Satellite Systems: Insights into GPS, GLONASS, Galileo, Compass and Others*. CRC Press; first edition, 2011.

[11] A. El-Rabbany. *Introduction to GPS: The Global Positioning System*. Artech House, 2002.

[12] K. Roebruck. *Glonass High-Impact Strategies - What You Need to Know : Definitions, Adoptions, Impact, Benefits, Maturity, Vendors*. Emereo Pty Limited, 2011.

[13] I. Petrovski. *GPS, Glonass, Galileo, and Beidou for Mobile Devices: From Instant to Precise Positioning*. Cambridge University Press, 2014.

[14] European Commision. http://ec.europa.eu/enterprise/policies/satnav/index_en.htm, opened on 14/04/14.

[15] European Comission. Regulation (EC) No 683/2008 of 9 July 2008 on the further implementation of the European satellite navigation programmes (EGNOS and Galileo), 2008.

[16] D. Skournetou. *Delay Estimators For Tracking Low CNR GNSS Signals*. Master thesis, Tampere University of Technology, 2007.

[17] N. C. Shivaramaiah and A. G. Dempster. The Galileo E5 AltBOC: Understanding the Signal Structure. In *International Global Navigation Satellite Systems Society Symposium 2009*, Surfers Paradise, Australia, December 2009. IGNSS Society.

[18] M. S. Yarlykov. The statistical characteristics of navigation cosine binary offset carrier modulated signals (CosBOC signals). *Journal of Communications Technology and Electronics*, volume 55(9):pages 990–1004, January 2010.

[19] T. Saxena, M. Tech, and J. S. Jadon. Spectral analysis of Sine and Cosine BOC modulated signals. In *2014 International Conference Signal Processing of Integrated Networks*, pages 734–738, Noida, India, February 2014. IEEE.

[20] J. Zhang. *Advanced signal processing in multi-mode multi-frequency receivers for positioning applications*. PhD thesis, Tampere University of Technology, 2013.

[21] A. Lohan, E. S. Burian and M. Renfors. Low-complexity aqcuisition methods for split spectrum CDMA signals. *Wiley International Journal of Satellite Communications*, volume 26:pages 503–522, October 2008.

[22] G.W. Hein, J.-A. Avila-Rodriguez, S. Wallner, A.R. Pratt, J. Owen, J. Issler, J.W. Betz, C.J. Hegarty, S. Lenahan, J.J. Rushanan, A.L. Kraay, and T.A. Stansell. MBOC: The New Optimized Spreading Modulation Recommended for GALILEO L1 OS and GPS L1C. In *Position, Location, And Navigation Symposium, 2006 IEEE/ION*, pages 883–892, Fort Worth, USA, April 2006. IEEE.

[23] E. Rebeyrol, C. Macabiau, M. Lestarquit, M. L. Boucheret, and M. Bousquet. BOC power spectrum densities. In *Proceedings of the 2005 National Technical Meeting of The Institute of Navigation*, pages 769–788, San Diego, USA, January 2005. ION.

[24] J. B. Y. Tsui. *Fundamentals of global positioning systems receivers: A software approach*. Wiley Interscience, second edition, 2005.

[25] G.W. Hein, J.-A. Avila-Rodriguez, and S. Wallner. The Galileo Code and Others. *Inside GNSS*, pages 62–74, September 2006.

[26] E. Re and M. Ruggieri. *Satellite Communications and Navigation Systems, url = http://books.google.com/books?id=xb_vpXN_frEC&pgis=1, year = 2007*. Springer.

[27] L. R. Weill. Differences between Signal Acquisition and Tracking . *Inside GNSS*, pages 22–27, February 2011.

[28] E. S. Lohan. Statistical analysis of BPSK-like techniques for the acquisition of Galileo signals. *AIAA Journal of Aerospace Computing, Information, and Communication*, 3:234–243, May 2005.

[29] A. Polydoros and C. Weber. A Unified Approach to Serial Search Spread-Spectrum Code Acquisition–Part I: General Theory. *IEEE Transactions on Communications*, volume 32(5):pages 542–549, May 1984.

[30] D.J.R. van Nee and A.J.R.M. Coenen. New fast GPS code-acquisition technique using FFT. *Electronics Letter*, volume 27(2):pages 158–160, January 1991.

[31] A. Burian, E. S. Lohan, and M. Renfors. BPSK-like Methods for Hybrid-Search Acquisition of Galileo Signals. In *2006 IEEE International Conference on Communications*, volume 11, pages 5211–5216, Istanbul, Turkey, June 2006. IEEE.

[32] P. Misra and P. Enge. *Global positioning system: signals, measurements, and performance*. Ganga-Jamuna Press, second edition, 2006.

[33] E. S. Warner and J. D. Last. Interpretation of s-curve and tracking error in a delay-lock-loop. *Journal of Navigation*, volume 48:pages 303–306, May 1995.

[34] A. J. Van Dierendonck, P. Fenton, and T. Ford. Theory and Performance of Narrow Correlator Spacing in a GPS Receiver. In *Proceedings of the 1992 National Technical Meeting of The Institute of Navigation*, pages 115–124, San Diego, USA, January 1992. ION.

[35] K. Rouabah, D. Chikouche, F. Bouttout, R. Harba, and P. Ravier. GPS/-Galileo Multipath Mitigation Using the First Side Peak of Double Delta Correlator. *Wireless Personal Communications*, volume 60(2):pages 321–333, March 2010.

[36] G. A. McGraw and M. S. Braasch. GNSS Multipath Mitigation Using Gated and High Resolution Correlator Concepts. In *Proceedings of the 1999 National Technical Meeting of The Institute of Navigation*, pages 333–342, San Diego, USA, January 1999. ION.

[37] M.K. Simon, J.K. Omura, R.A. Scholtz, and B.K. Levit. *Spread Spectrum Communication Handbook*. McGraw-Hill, NewYork, USA, revised edition, 1994.

[38] D.P. Taylor. Introduction to "Synchronous Communications". *Proceedings of the IEEE*, volume 90:pages 1459–1460, August 2002.

[39] C.H. Yinger, W.A. Feess, V. Nuth, and R.N. Haddad. GPS Accuracy Versus Number of NIMA Stations. In *Proceedings of the 16th International Technical Meeting of the Satellite Division of The Institute of Navigation (ION GPS/GNSS 2003*, pages 1526–1533, Portland, USA, September 2003. ION.

[40] K. Yu, I. Sharp, and Y. J. Guo. *Ground-Based Wireless Positioning*. John Wiley & Sons, 2009.

[41] H. Suda and H. Kobayashi. On time-of arrival positioning in a multipath environment. In *Vehicular Technology Conference, 2004. VTC2004-Fall. 2004 IEEE 60th*, volume 7, pages 3540–3544, Los Angeles, USA, September 2004. IEEE.

[42] J. S. Isaac Amundson. RF angle of arrival-based node localisation. *International Journal of Sensor Networks*, volume 9:pages 209 – 224, May 2011.

[43] M. Bouet and A. L. dos Santos. RFID tags: Positioning principles and localization techniques. In *Wireless Days, 2008. WD '08. 1st IFIP*, pages 1–5, Dubai, November 2008. IEEE.

[44] D. M. Franco-Patino, G. Seco-Granados, and F. Dovis. Signal quality checks for multipath detection in GNSS. In *2013 International Conference on Localization and GNSS (ICL-GNSS)*, pages 1–6, Turin, Italy, June 2013. IEEE.

[45] P. D. Groves, Z. Jiang, M. Rudi, and P. Strode. A Portfolio Approach to NLOS and Multipath Mitigation in Dense Urban Areas. In *Proceedings of the 26th International Technical Meeting of The Satellite Division of the Institute of Navigation (ION GNSS+ 2013)*, pages 3231–3247, Nashville, USA, September 2013. ION.

[46] M. Irsigler and G. W. Hein. Development of a Real-Time Multipath Monitor Based on Multi-Correlator Observations. In *Proceedings of the 18th International Technical Meeting of the Satellite Division of The Institute of Navigation (ION GNSS 2005)*, pages 2626–2637, Long Beach, USA, September 2005. ION.

[47] P. Closas and C. Fernandez-Prades. A Statistical Multipath Detector for Antenna Array Based GNSS Receivers. *IEEE Transactions on Wireless Communications*, volume 10(3):pages 916–929, March 2011.

[48] J. Borras, P. Hatrack, and N.B. Mandayam. Decision theoretic framework for NLOS identification. In *VTC '98. 48th IEEE Vehicular Technology Conference*, volume 2, pages 1583–1587, Ottawa, Canada, May 1998. IEEE.

[49] K. Yu, I. Sharp, and Y. J. Guo. Ground-Based Wireless Positioning. In *Wiley-IEEE Press*, page 450, 2009.

[50] J. Riba and A. Urruela. A non-line-of-sight mitigation technique based on ML-detection. In *Speech, and Signal Processing, 2004. Proceedings. (ICASSP '04). IEEE International Conference on Acoustics*, volume 2, pages ii–153–6, Montreal, Canada, May 2004. IEEE.

[51] F. Montorsi, F. Pancaldi, and G. M. Vitetta. Statistical Characterization and Mitigation of NLOS Bias in UWB Localization Systems. *Advances in Electronics and Telecommunications*, pages 11–17, March 2012.

[52] S. Peyraud, D. Bétaille, S. Renault, M. Ortiz, F. Mougel, D. Meizel, and F. Peyret. About non-line-of-sight satellite detection and exclusion in a 3D map-aided localization algorithm. *Sensors 2013*, volume 13:pages 829–847, January 2013.

[53] P. D. Groves, Z. Jiang, L. Wang, and M. K. Ziebart. Intelligent Urban Positioning using Multi-Constellation GNSS with 3D Mapping and NLOS Signal Detection. In *Proceedings of the 25th International Technical Meeting of The Satellite Division of the Institute of Navigation (ION GNSS 2012))*, pages 458–472, Nashville, USA, September 2012. ION.

[54] L. Wang, P.D. Groves, and M.K. Ziebart. Urban Positioning on a Smartphone: Real-time Shadow Matching Using GNSS and 3D City Models. In *Proceedings of the 26th International Technical Meeting of The Satellite Division of the Institute of Navigation (ION GNSS 2013)*, pages 1606–1619, Nashville, USA, September 2013. ION.

[55] M. Liso Nicolas, M. Jacob, M. Smyrnaios, S. Schon, and T. Kurner. Basic concepts for the modeling and correction of GNSS multipath effects using ray tracing and software receivers. In *Antennas and Propagation in Wireless Communications (APWC), 2011 IEEE-APS Topical Conference on Antennas and Propagation in Wireless Communications (APWC)*, pages 890–893, Torino, Italy, September 2011. IEEE.

[56] S. Bauer, M. Obst, R. Streiter, and G. Wanielik. Evaluation of Shadow Maps for Non-Line-of-Sight Detection in Urban GNSS Vehicle Localization with VANETs - The GAIN Approach. In *Vehicular Technology Conference (VTC Spring), 2013 IEEE 77th*, pages 1–5, Dresden, Germany, June 2013.

[57] L. Wang, P.D. Groves, and M.K. Ziebart. Urban Positioning on a Smatphone. *Inside GNSS*, pages 44 – 57, December 2013.

[58] G. Giunta and L. Vandendorpe. A "rayleigh-ness" test for DS/SS code acquisition. *IEEE Transactions on Communication*, volume 51(9):pages 1492–1501, September 2003.

[59] G. Benedetto, F.and Giunta. LOS/NLOS DETECTION BY THE NORMALIZED RAYLEIGH-NESS TEST. In *17th European Signal Processing Conference*, pages 2131–2135, Glasgow, Scottland, August 2009.

[60] W.R. Braun. PN acquisition and tracking performance in DS/CDMA systems with symbol-length spreading sequences. *IEEE Transactions on Communications*, volume 45(12):pages 1595–1601, December 1997.

[61] M. Z. H. Bhuiyan, J. Zhang, E. S. Lohan, W. Wang, and S. Sand. Analysis of Multipath Mitigation Techniques with Land Mobile Satellite Channel Model. *Radioengineering*, volume 21(4):pages 1067–1077, December 2012.

[62] W. Betz, J and K. R. Kolodziejski. Extended theory of early-late code tracking for a bandlimited GPS receiver. *Navigation: Journal of the Institute of Navigation*, volume 47(3):pages 211–226, September 2000.

[63] M. Irsigler and B. Eissfeller. Comparison of Multipath Mitigation Techniques with Consideration of Future Signal Structures. In *Proceedings of the 16th International Technical Meeting of the Satellite Division of The Institute of Navigation*, pages 2584–2592, Portland, USA, September 2003. ION.

[64] E. S. Lohan, R. Hamila, A. Lakhzouri, and M. Renfors. Highly efficient techniques for mitigating the effects of multipath propagation in DS-CDMA delay estimation. *IEEE Transactions on Wireless Communications*, volume 4(1):pages 149–162, January 2005.

[65] E. S. Lohan, R. Hamila, and M. Renfors. Performance analysis of an efficient multipath delay estimation approach in a CDMA multiuser environment. In *12th IEEE International Symposium on Personal, Indoor and Mobile Radio Communications*, volume 1, pages A–6–A–10, San Diego, USA, September 2001. IEEE.

[66] M. Z. H. Bhuiyan, E. S. Lohan, and M. Renfors. Code Tracking Algorithms for Mitigating Multipath Effects in Fading Channels for Satellite-Based Positioning. *EURASIP Journal on Advances in Signal Processing*, volume 2008(1):pages 1–18, November 2008.

[67] J. Aldrich. R.A. Fisher and the making of maximum likelihood 1912-1922. *Statistical Science*, volume 12(3):pages 162–176, August 1997.

[68] E.L. Lehmann and G. Casella. *Theory of Point Estimation*. Springer Texts in Statistics. Springer, second edition, 1998.

[69] R.D.J. van Nee, J. Siereveld, P.C. Fenton, and B.R. Townsend. The multipath estimating delay lock loop: approaching theoretical accuracy limits.

In *IEEE Position Location and Navigation Symposium*, pages 246–251, Las Vegas, USA, April 1994. IEEE.

[70] M. Z. H. Bhuiyan and E. S. Lohan. Advanced Multipath Mitigation Techniques for Satellite-Based Positioning Applications. *International Journal of Navigation and Observation*, volume 2010:pages 15, January 2010.

[71] A. Papoulis and S. U. Pillai. *Probability, Random Variables, and Stochastic Processes*. Tata McGraw-Hill, 2002.

[72] N. Youssef, T. Munakata, and M. Takeda. Fade statistics in Nakagami fading environments. In *IEEE 4th International Symposium on Spread Spectrum Techniques and Applications Proceedings*, volume 3, pages 1244–1247, Mainz, Germany, September 1996. IEEE.

[73] W. C. Jakes. *Microwave mobile communications*. Wiley-IEEE Press, revised edition, 1994.

[74] M. Stefanovic, A. Mitic, and D. Pavlovic. The comparation of the signal statistical characteristics for various combining techniques in the Weibull fading channel. *INFOTEH*, March 2007.

[75] M. Stefanovic, D. Krstic, S. Panic, and Z. Popovic. Level Crossing Rate and Average Fade Duration of SC macrodiversity system over independent Hoyt fading channels. In *17th International Conference on Software, Telecommunications & Computer Networks*, pages 239–243, Hvar, Croatia, September 2009. IEEE.

[76] A.A. Abu-Dayya and N.C. Beaulieu. Outage probabilities of cellular mobile radio systems with multiple Nakagami interferers. *IEEE Transactions on Vehicular Technology*, volume 40(4):pages 757–768, November 1991.

[77] A. Shah and A.M. Haimovich. Performance analysis of maximal ratio combining and comparison with optimum combining for mobile radio communications with cochannel interference. *IEEE Transactions on Vehicular Technology*, volume 49(4):pages 1454–1463, July 2000.

[78] L. Yang and M.-S. Alouini. On the Average Outage Rate and Average Outage Duration of Wireless Communication Systems With Multiple Cochannel Interferers. *IEEE Transactions on Wireless Communications*, volume 3(4):pages 1142–1153, July 2004.

[79] J. Mark and W. Zhuang. *Wireless Communications and Networking*. Prentice Hall, 2003.

[80] J.-P. M. G. Linnartz and R. Prasad. Threshold crossing rate and average non-fade duration in a Rayleigh-fading channel with multiple interferers. *Archiv fuer Elektronik und Uebertragungstechnik (ISSN 0001-1096)*, volume 43:pages 345–349, December 1989.

[81] A. Emad and N. C. Beaulieu. Performance of an AFC Loop in the Presence of a Single Interferer in a Fading Channel. *IEEE Transactions on Communications*, volume 58(12):pages 3386–3391, December 2011.

[82] K.W. Sowerby and A.G. Williamson. Outage probability calculations for multiple cochannel interferers in cellular mobile radio systems. volume 135(3):pages 208–215, November 1988.

[83] A.A. Abu-Dayya and N.C. Beaulieu. Outage probabilities of cellular mobile radio systems with multiple Nakagami interferers. *IEEE Transactions on Vehicular Technology*, volume 40(4):pages 757–768, November 1991.

[84] W. C. Y. Lee. *Mobile communications engineering: theory and applications*. McGraw-Hill, 1998.

[85] C.-D. Iskander and P. Takis Mathiopoulos. Analytical level crossing rates and average fade durations for diversity techniques in Nakagami fading channels. *IEEE Transactions on Communications*, volume 50(8):pages 1301–1309, August 2002.

[86] D.G. Brennan. Linear diversity combining techniques. *Proceedings of the IEEE*, volume 91(2):pages 331–356, February 2003.

[87] Hong-Chuan Yang. New results on ordered statistics and analysis of minimum-selection generalized selection combining (GSC). *IEEE Transactions on Wireless Communications*, volume 5(7):pages 1876–1885, July 2006.

[88] M. O. Hasna and M. S. Alouini. A Performance Study of Dual-Hop Transmissions With Fixed Gain Relays. *IEEE Transactions on Wireless Communications*, volume 3(6):pages 1963–1968, November 2004.

[89] M. O. Hasna and M. S. Alouini. Outage probability of multihop transmission over Nakagami fading channels. *IEEE Communications Letters*, volume 7(5):pages 216–218, May 2003.

[90] M. O. Hasna and M. S. Alouini. Average outage duration of multihop communication systems with regenerative relays. *IEEE Transactions on Wireless Communications*, volume 4(4):pages 1366–1371, July 2005.

[91] Z. Hadzi-Velkov, N. Zlatanov, and G. K. Karagiannidis. Level Crossing Rate and Average Fade Duration of the Multihop Rayleigh Fading Channel. In *2008 IEEE International Conference on Communications*, pages 4451–4455, Beijing, China, May 2008. IEEE.

[92] M. O. Hasna and M. S. Alouini. Outage probability of multihop transmission over Nakagami fading channels. *IEEE Communications Letters*, volume 7(5):pages 216–218, May 2003.

[93] A. Schmid and A. Neubauer. Carrier to Noise Power Estimation for Enhanced Sensitivity Galileo/GPS Receivers. In *IEEE 61st Vehicular Technology Conference*, volume 4, pages 2629–2633, Stockholm, Sweden, June 2005. IEEE.

[94] C. Tepedelenlioglu, A. Abdi, G. B. Giannakis, and M. Kaveh. Estimation of Doppler spread and signal strength in mobile communications with applications to handoff and adaptive transmission. *Wireless Communications and Mobile Computing*, volume 1(2):pages 221–242, April 2001.

[95] K. Ramasubramanian and S. Nadig. Performance Bounds for Carrier-to-Noise Ratio Estimation in GPS Receivers. In *Proceedings of the 2006 National Technical Meeting of The Institute of Navigation*, pages 953–957, Monterey, Canada, January 2006. ION.

[96] D. Skournetou. *Mitigation of Dominant Channel Propagation Effects in GNSS-based Positioning*. PhD thesis, Tampere University of Technology, 2011.

[97] D. Skournetou and E. S. Lohan. Indoor location awareness based on the non-coherent correlation function for gnss signals. In *Finish Signal Processing Symposium*, Oulu, Finland, August 2007.

[98] E. S. Lohan and D. Skournetou. Level Crossing Rate Estimation (LCRE). *Inside GNSS*, pages 36–47, September 2010.

[99] A. K. M. N. Islam. *CNR estimation and indoor channel modeling of GPS signals*. PhD thesis, Tampere University of Technology, April 2008.

[100] A. K. M. N. Islam, E. S. Lohan, and M. Renfors. Moment based CNR estimators for BOC/BPSK modulated signal for Galileo/GPS. In *5th Workshop on Positioning, Navigation and Communication*, pages 129–136, Hannover, Germany, March 2008. IEEE.

[101] D.J. Brooks and J.A. Chambers. Multi-branch DFE for Rayleigh fading multipath channels. *Electronics Letters*, volume 33(18):pages 1537–1538, August 1997.

Appendices

A Matlab script of the local maxima search

```
function [number] = Find_local_maxmin( F,lv,c,CNR )
% Function search for near local maximum and minimum and
% avoid crossings under a specific threshold
% Input:
% - F       =   ACF
% - lv      =   Level of LCR
% - c       =   Position of zero-crossing of LCR
% - CNR     =   Current CNR, which has to be estimated in
%               before
% Output:
% - number  =   LCR counts with respect to the level and
%               threshold
% By Denis Surmann, 04.06.2014

a = zeros(length(c)-1,1);

%% Detection of local maxima and minima
%  between the zero crossing at level lv
for i=1:1:length(c)-1,

    c1 = c(i);
    c2 = c(i+1);

if      abs(c1-c2) == 1,
        a(i,:) = F(1,c2);
else    max_F = max(F(1,c1+1:c2));
        min_F = min(F(1,c1+1:c2));
```

```
        if max_F > lv,
        a(i,:) = max_F;
        else
        if min_F < lv,
        a(i,:) = min_F;
        end;
        end;
end;
end;

%% Treshold
% Threshold is created by the knowledge of the tests, that had
% been done before
if CNR <= 25
      thresh = 2.286*10^(-4)*CNR^2-4.343*10^(-3)*CNR+...
      6.457*10^(-2);
      else
      if CNR <=32.5
      thresh = -1.067*10^(-4)*CNR^3+8.8*10^(-3)*CNR^2-...
      2.453*10^(-1)*CNR+2.4;
      else
      thresh = 4*10^(-4)*CNR^2-3.58*10^(-2)*CNR+8.015*...
      10^(-1);
      end;
end;

%% Decision of use
% If the maxima and minima between the crossings are over
% the threshold, they are saved in following vector b,
% otherwise not

b = 0;
for i=1:length(a),
    if i > 1,
    if i == length(a),
       if (abs(a(i-1)-a(i)) > thresh)
```

```
            b(i,:) = c(i);
        else
            b(i,:) = 0;
        end;
        else
            if (abs(a(i-1)-a(i)) > thresh || abs(a(i)-...
                a(i+1)) > thresh),
                b(i,:) = c(i);
            else
            b(i,:) = 0;
            end;
    end;
    else
        if length(a) > 1,
            if (abs(a(i)-a(i+1)) > thresh),
            b(i,:) = c(i);
            else
            b(i,:) = 0;
            end;
        else
            number = 1;
        end;
    end;
end;

% Fill 0 in the output, if there are no LCRs under the
% threshold
if b == 0,
   number = 0;
else
   number = length(find(b>0));
end;
```

B Matlab script of the multipath detector

```
function [m] = Multipath_detection(ACF_lv, lcr, CNR)
%This function identifies whether the NLOS signal is one-
%or multipath with use of a normal distribution
% Input:
% - lcr (number of level crossings)
% - CNR (Signal to Noise Ratio)
% - ACF_lv  (Level of ACF function)
% Output: m (One path = 0, Multipath = 1)
% Created by Denis Surmannn 19.06.2014

%% Estimate the parameter for the normal distribution
f = 3.476*10^(-2)*CNR^2-3.82*CNR+1.054*10^2;
  if CNR <=27.5
      sigma = 20;
      mu = 330;
  else
      if CNR <= 32.5
      sigma = 5.2*10^(-1)*CNR^2-2.950*10^(1)*CNR+4.38*10^2;
      mu = -4.444*10^(-02)*CNR^3 + 4.171*CNR^2 - 1.312*...
          10^(02)*CNR + 1.706*10^(03);
      else
      sigma = -2.8*10^(-1)*CNR^2+2.326*10^(1)*CNR-4.32*10^2;
      mu = -4.444*10^(-02)*CNR^3 + 4.171*CNR^2 - 1.312*...
          10^(02)*CNR + 1.706*10^(03);
      f = -6*10^(-2)*CNR^2+2.69*CNR-6.575;
      end;
  end;
```

```
%% Detection
% In here, the normal distribution is created: If the ACF
% level is under the threshold, probably one-path is
% detected with m = 0, otherwise multipath is detected so
% that m = 1

for n = 1:length(lcr)
    marker = normpdf(lcr(n,:),mu,sigma)*f;
if (ACF_lv(n) <= marker)
   m(n) = 0;
else
   m(n) = 1;
end;
end;

%% Plot
start_x = lcr-100;
end_x = lcr+100;
xax = start_x:end_x;
curfct= normpdf(xax,mu,sigma)*f;
plot(xax,curfct, 'b', 'LineWidth', 3); hold on;
plot(lcr, ACF_lv, 'r*'); hold on; grid on;
legend('Distribution Curve', 'Measured LCR');
xlim([start_x end_x]);
ylim([0 max(max(curfct))*2]);
ylabel('Level of ACF');
xlabel('Number of crossings')
end
```